The Institute of Space and Astronautical Science
Report No. 638, March 1991

Hot Wire Measurement of Cross-linking and Unlinking in Uniting Two Circular Vortex Rings

Naoki IZUTSU* and Yuko OSHIMA**[1]

The Institute of Space and Astronautical Science
3-1-1, Yoshinodai, Sagamihara-shi, Kanagawa 229, Japan
**Faculty of Science, Ochanomizu University
2-1-1, Otsuka, Bunkyo-ku, Tokyo 112, Japan

Abstract

A laminar circular vortex ring with excellent reproducibility can be generated by pushing a mass of air through a circular orifice drilled on a buffer plate placed in front of a loudspeaker, which is driven by a stepwise voltage signal. In order to obtain complete information concerning the velocity fields during the 'uniting' of two circular vortex rings, phase-locked velocity measurement was carried out by using a single inclined hot wire point by point all over the flow field, and the vorticity fields were computed from the measured velocity fields. The vortex tubes representing the vortex rings were computed as well as the behavior of the fluid material initially held within the vortex ring, and the important differences among the vorticity, vortex tubes, and fluid material being transported by following the velocity field were explained so as not to misread the real phenomenon and the substance of the physical mechanism. The through process can be divided into the terms of formation & approaching, first cross-linking & unlinking, second cross-linking & unlinking and decay. The first cross-linking & unlinking is 'positive' and finishes successfully by the continuous and increasing driving force on the adjoined original 'near' segments being pressed against each other, while the second cross-linking & unlinking is 'negative' and depends on the initial condition due to the monotonously decreasing driving force on the adjoined original 'far' segments in the united vortex ring. As the continuous induced velocities on the approaching and adjoining segments force the segments harder against each other, the flow region in their gap is narrowed, and immediately after the gap cannot hold the whole flux the flow overflows outward to create another velocity gradient that is observed as the sudden appearance of two new concentrated vorticity regions between the adjacent vortex tubes. Therefore, the vorticity in the adjoined original vortex tubes is transported, although no vorticity cancellation is recognized in the present measurement because the time scale of cancellation is much longer than that of the cross-linking & unlinking. Moreover, several regulations for the quantitative description of the cross-linking & unlinking process were derived to obtain the time scale in addition to the progress rate of the uniting. Furthermore, the 'tail' parts of the fluid material are observed both during the isolating phase after the formation of the vortex rings and from the 'pull out' phase in the second cross-linking & unlinking through the decay phase. The 'cap' of the fluid material is observed during the second cross-linking & unlinking phase that originates in the accumulated fluid material around the neutral center line in the first cross-linking & unlinking. Both the 'tail' and the 'cap' have no vorticity although the 'trail' appearing in the formation process has vorticity.

[1]Present address : Research and Development Center, Ricoh Co.Ltd., 16-1, Shin'ei-cho, Kohoku-ku, Yokohama 223, Japan.

1. INTRODUCTION

Transformations and interactions of concentrated vorticity regions in an unbounded space are fundamental aspects of fluid dynamics. In two dimensional flow, vorticity is scalar and the interactions between two circular vortices are sorted into two major groups. One is the merging of two vortices with the same directions of rotation as sketched in Fig. 1(a) and the other is the cancellation between a positive vortex and a negative in Fig. 1(b). Each group has various patterns of interaction depending on the strength (or Reynolds number), distance and structure of the vortices. In three-dimensional flow, vorticity is a vector and forms a vortex tube as assembling the vorticity lines. So-called cross-linking and unlinking in addition to merging and cancellation can happen between two adjacent vortex tubes due to their local curvatures, and these interactions can be said to be a basic phenomena characterizing vortex dynamics. The most typical and simple situation of a vortex tube is a free laminar circular vortex ring, which can be easily observed through flow visualization and is stably reproduced in laboratory experiments by single or intermittent ejection of a fluid mass through a circular opening.

Interactions between two free laminar circular vortex rings are classified into four classes by their final approaching styles as illustrated in Fig. 2. The interaction between two vortex rings moving in the same directions along their common axis as shown in Fig. 2(a) is called as 'passing through'. Well-known leapfrogging games can happen several times and their last stage is the merging of them. In Fig. 2(b), the interaction between two vortex rings moving along their collision courses is known as the 'head-on collision' case. They spread out

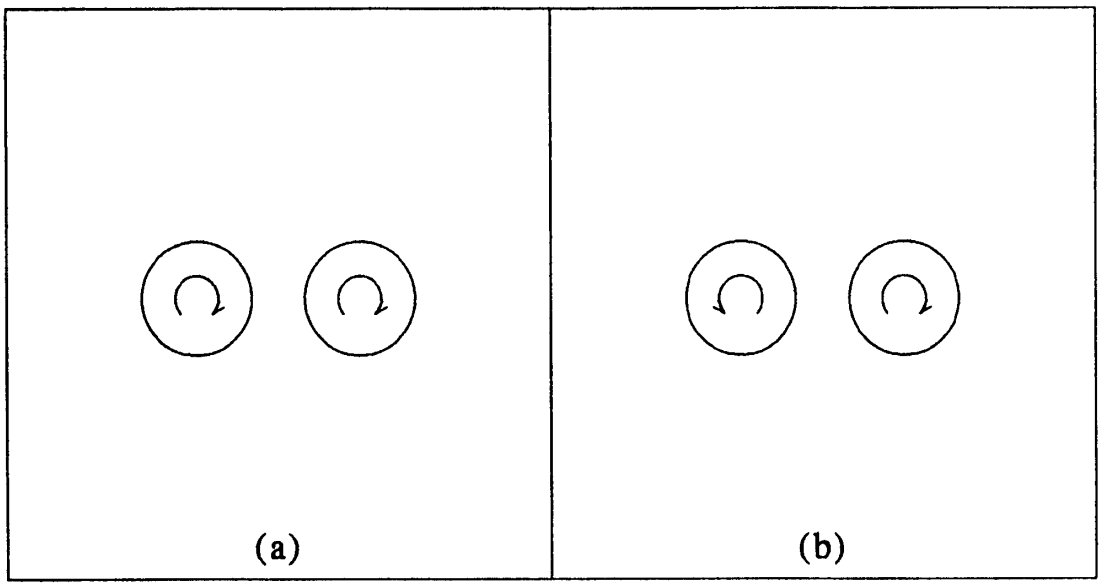

Fig.1 Two-dimensional interactions of two circular vortices are illustrated in (a) merging and (b) cancellation, an arrow indicates the direction of rotation.

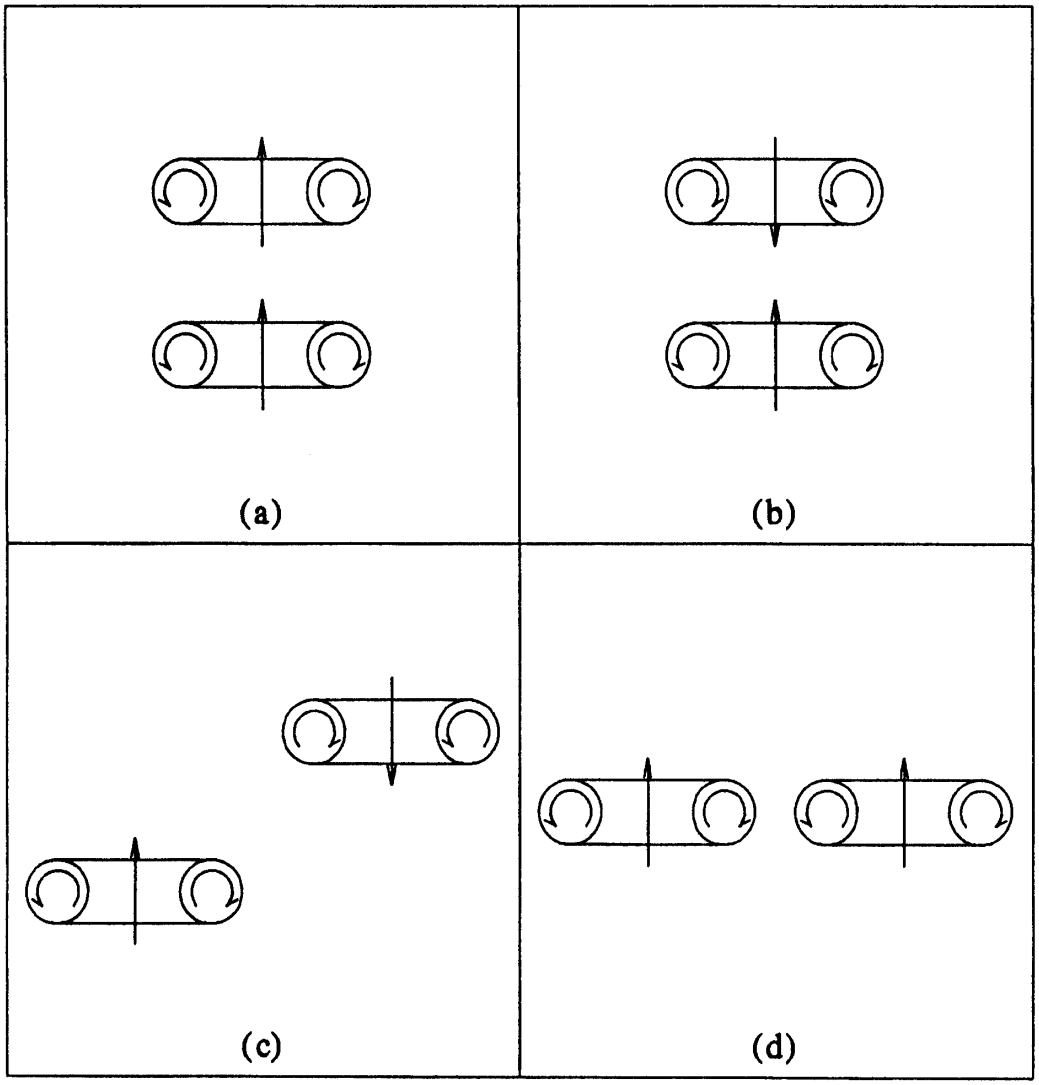

Fig.2 Four classes of the final approaching styles in two circular vortex rings ; (a) 'passing through' and 'merging', (b) 'head-on collision' and 'cancellation', (c) 'passing each other' (d) 'uniting'.

and can be canceled in their final step. If the axes of two vortex rings do not coincide and are at a moderate distance apart, three-dimensional interactions occur between the rings. When the traveling directions of approaching vortex rings are opposite as seen in Fig. 2(c), the vorticity regions with same senses have first interaction by attracting each other. It is classified as the 'passing each other' case and the complicated phenomenon is predicted. Figure 2(d) shows the last class, in which the interaction between two vortex rings moving in the same directions is played. First interaction and then 'uniting' occurs in the contact region with the adjoining parts of the vortex rings with opposite senses. This phenomenon was studied in this paper. The term 'uniting' in Fig. 2(d) is used for the process without 'merging', which means that two vortex tubes with

same senses simply become one vortex tube such as the patterns of Figs. 1(a) and 2(a).

The observation by direct flow visualization has made us believe that two vortex rings proceeding side by side come close to each other by their mutual induced velocities, and that they make contact with a finite final approaching angle before they unite into a single distorted vortex ring through 'cross-linking' between the two vortex rings and 'unlinking' of the adjoining parts of the original rings. The united ring splits again into two new vortex rings under the specific conditions. The experimental work of the two vortex rings ejected from coplanar circular orifices was made in water by the flow visualization method using two colors by Oshima & Asaka (1975) and the existence of the cross-linking phenomena of the vortex tubes was reported Reynolds number about 400 defined by the orifice diameter and the speed of the vortex rings. They also discovered another 'splitting' of the united vortex ring. The term 'splitting' is used for the process by which a vortex ring becomes several new independent vortex rings. Fohl & Turner (1975) investigated the same phenomena in water through the two color dye visualization technique at Reynolds number about 3000 defined by the speed of the vortex ring and the ring diameter. They examined the effect of the approaching angle, which is defined as the half crossing angle of the axes of the rings, from 5° through 30° and concluded that an approaching angle greater than 16° always caused another splitting of the united vortex ring into two new vortex rings, and one less than 5° however resulted in no splittings. Oshima & Asaka (1977) investigated these phenomena in air by smoke visualization, where the Reynolds number was changed from 180 through 650 defined by the orifice diameter and the speed of the vortex ring. They also examined the effect of the ring interval ratio, the distance between the two orifices' centers to their diameter. This parameter is almost equivalent to the final approaching angle, if the Reynolds number is redefined by the property of the rings just before contact. Their conclusion was that a faster initial speed of the vortex rings causes another splitting from the united vortex ring. The reason is that the initial speed of the vortex ring determines the final approaching angle just before contact, in relation to the ring interval ratio. A faster initial speed of the vortex ring means a larger circulation of it same as a larger Reynolds number, thus the parameters describing this phenomenon can be said to be the final approaching vortex rings' circulations and their crossing angle. The core size of the vortex ring is certainly important, however we hardly have the freedom for determining the core size and its structure in laboratory experiments.

Schatzle (1987) carried out the velocity measurement in a water tank using a two-component laser-doppler velocimeter. The Reynolds number of his measurement was approximately 1600 defined as the circulation divided by the kinematic viscosity and the initial approaching angle of the rings was 7.5°. The vorticity fields computed from the measured velocity components showed the circulation disappearance in the contact region of the vortex rings, nevertheless he detected no obvious cross-linking process. Proof of the cross-linking process

between two vortex rings was discovered through the hot wire measurement by Oshima & Izutsu (1988). They utilized the fully automatic equipment for hot wire measurement and a computer graphical approach in order to detect the process of cross-linking and unlinking in two vortex rings. Their investigation as well as Schatzle's is based on the concept of mean flow grasp and the interacting regions are spatially discretized, where the phase-locked velocity measurements are carried out repeatedly point by point.

The rather common approach for studying the cross-linking phenomena has been that of numerical simulations and the incompressible Navier-Stokes equations have been numerically solved by many researchers. Ashurst & Meiron (1987) discovered numerically the existence of 'reconnection' depending on Reynolds numbers 10,100,1000 and 5000. Melander & Zabusky (1988) studied this phenomenon by spectral method with periodic boundary conditions. Kida, Takaoka & Hussain (1989) carried out in the Reynolds number of 578 with the approaching angle of 30° and found out another splitting situation of the united vortex ring. Kerr & Hussain (1989) also executed the simulation with the Reynolds number from 1600 through 3200, while Ishii, Hussain, Kuwahara & Liu (1989) studied by vector potential-vorticity method in the Reynolds number 62.8 and 628 with no approaching angle. In all the previous numerical simulations, initial conditions were set by assuming vorticity distributions such as the Gaussian form, then the velocity fields were calculated by integral under Biot-Savart law. Therefore the Reynolds number was defined by the circulation of the initial assumed vortex ring divided by the kinematic viscosity. On the contrary, the full simulations according to the real laboratory experiment were done by Chen (1991). His initial and boundary conditions were given by the velocity history on the circular openings, and the various physical quantities were computed for the understanding of this mechanism. Three-dimentional vortex method was applied by Noguchi (1986) and Leonard & Chua (1989). Those investigations were based on the motion of the vortex elements which were inviscid and acting on Lagrangian dynamics by Biot-Savart law. In order to get the cross-linking and unlinking of vortices, a core structure model and a cut-off mechanism in the adjoining zones must have been introduced artificially. On the other hand, 'a model of vortex reconnection' was proposed by Saffman (1990) to describe the breaking and rejoining of vortex lines based on the idea that viscosity cancels the vorticity where the filaments touch.

Although we found the existence of vorticity cross-linking and unlinking in the previous work, more precise and smaller scale measurements were necessary in order to clear up physically the cross-linking and unlinking phenomena. The possible difficulties in hot wire measurements were described in the paper of Izutsu & Oshima (1990) and a solution to this problem was worked out by using a single inclined hot wire with a rotation system and by using a computerized data processing system for determining the correct flow vectors including the reverse flow regions. In their paper, a new measuring system was developed and it was adapted to the various axisymmetric vortex ring cases, consequently the

ability for the precise measurement was assured. Because of the proof of the exactly symmetrical mean flow in this phenomenon, our measurement was concentrated in one quarter region of this flow field, as a result the mesh size could be relatively decreased.

Here, we must confirm the meaning of the terms such as 'cross-linking', 'unlinking', 'bridging', 'reconnection' and 'cut and connect' used by the preceding researchers. The process by which the new concentrated vorticity regions appear between the original two vortex tubes is called 'cross-linking' or 'bridging', which means there is no disappearance of the original vortex tubes. Because of the gradual growth of the newly created cross-linked vortex tubes, the adjoining parts of the original vortex tubes gradually weaken and finally disappear. This process is called as 'unlinking'. The uniting of the two vortex rings is accomplished by 'cross-linking' between the two vortex tubes and then 'unlinking' of the original vortex tubes, most of this process happening simultaneously. 'Reconnection' and 'cut and connect' of vortex tubes do not present this process pertinently because breaking the tubes follows connecting. Most researchers believe that the cross-linking and unlinking happen by cancellation of the vorticity in the contact region of the opposite vortex tubes, but the physically explained mechanism based on the real phenomenon has not yet been exposed. Our efforts were focused on the description of the real process of the cross-linking and unlinking in the two uniting vortex rings and its physical explanation.

The experimental system, hot wire technique, data processing procedure and experimental condition are explained in §2. The results appearing in §3 are divided into five subsections; the features on the planes of symmetry,the difference between vorticity and a vortex tube,the process of the first cross-linking and unlinking,the difference between vorticity and fluid material, and lastly the process of the second cross-linking and unlinking. The physical mechanism in the uniting of two vortex rings is summarized together with its throughout process in §4.

2. Measurement

2.1 Experimental system

The experimental equipment illustrated in the schematic of Fig. 3 for the present study is the same as was used in the paper of Izutsu & Oshima (1990) except that the orifice block was replaced by the new one. A vortex ring is generated by pushing an air mass out of a circular orifice made on a buffer plate in front of a 30cm loudspeaker, which is periodically driven by a step in electric signal. The two orifices of 0.8cm in radius, with centers placed 3.2cm apart, i.e. four times the radius, are used and their inner corners are rounded in order to keep the vortex formation stable and of good reproducibility. A 45° inclined hot wire probe is traversed in the measurement region over the orifices. A measurement system is composed of a three dimensional traverse unit, a probe

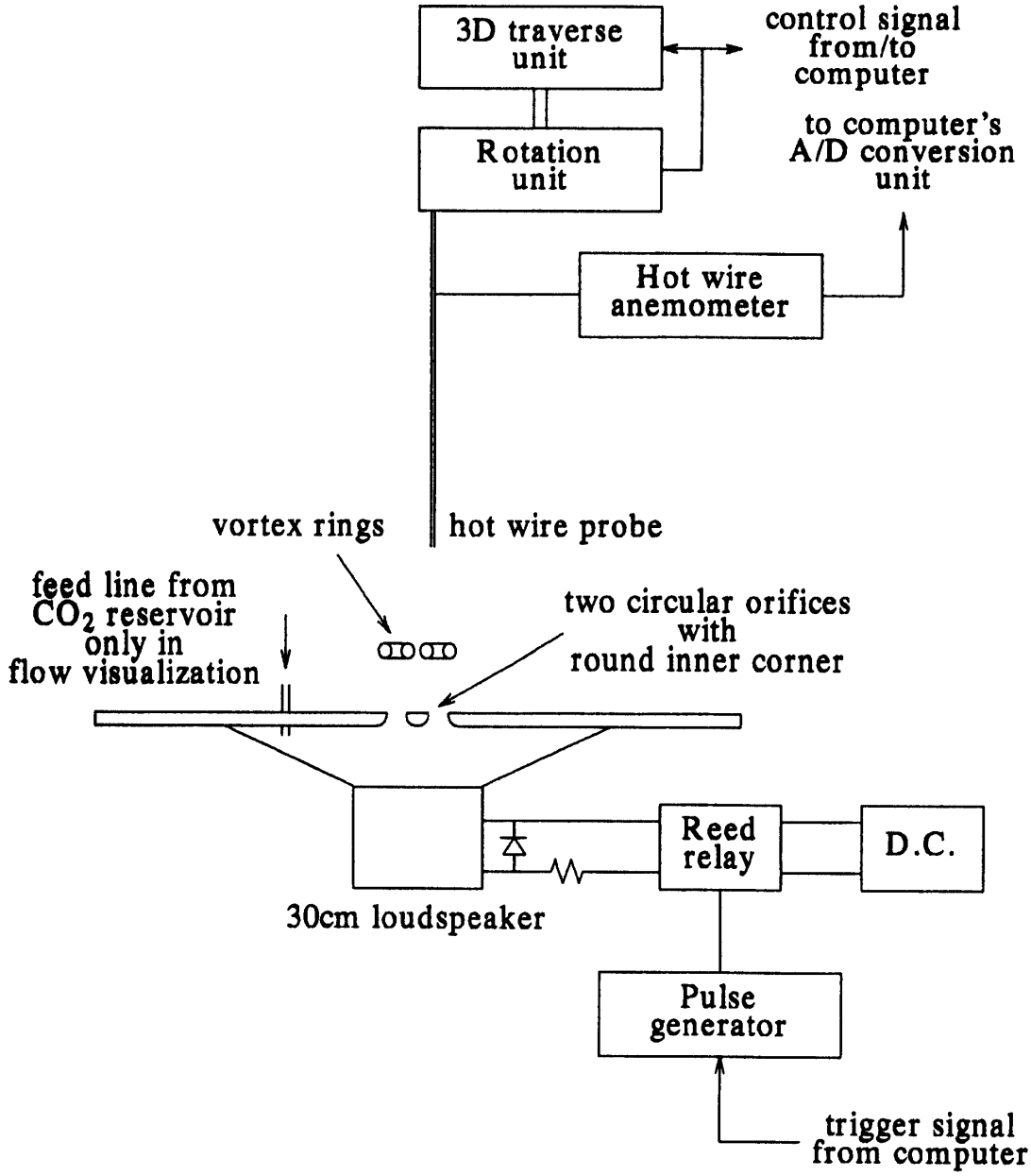

Fig.3 Experimental apparatus; the equipment consists of a three dimensional traverse unit, a probe rotation unit, a data acquisition unit, a relay unit and flow visualization system.

rotation unit, a data acquisition unit and a relay unit linked with a pulse generator. The data acquisition unit consists of a hot wire anemometer and an A/D conversion system. For flow visualization by Schlieren method, carbon dioxide gas can be fed into the primary jet through the enclosure of the loudspeaker. The visualization system consists of a CCD camera, image memory system, and a delay circuit unit, which operates a strobe light. They are also linked to the vortex generation system. The measurement and visualizing systems are controlled by a laboratory computer.

Figure 4 shows the cartesian coordinate system (x, y, z) and the configuration of the orifices.Two circular vortex rings with the same properties start to move upward with the speed of U, which is obtained at the centroid and is a function of the time t. The origin of the coordinates is fixed at the middle point between the circular orifices, whose radii are the same, denoted by R_o. The distance between the orifice centers is indicated by D_o and is $4D_o$ in the present case. The z-axis is taken perpendicularly to the openings plane. The x-axis is taken along the line including the centers of the orifices and the y-axis is at right angle to both the z-axis and x-axis. The velocity vector is indicated by the boldface symbol v and its components are presented by v_x, v_y and v_z, respectively. The velocity norm is denoted by v as

$$v=\sqrt{v_x{}^2+v_y{}^2+v_z{}^2}. \tag{1}$$

The trigger pulse applied to the relay unit was chosen as the base time $(t=0)$ for phase locked data acquisition. Checking the visualized images and the hot wire response signals, the amplitude and duration of a voltage pulse supplying to the loudspeaker were carefully adjusted so as to produce stable laminar vortex rings with good reproducibility. The period of the vortex generation was determined on the value of more than $100R_o/U$ to prevent any interaction between the rings and any disturbance.

The hot wire technique used in the present measurement is the same as was used by Izutsu & Oshima (1990). The total of 16 effective velocity data sets at every 22.5° angle of rotation were A/D converted repeatedly 8 times to be

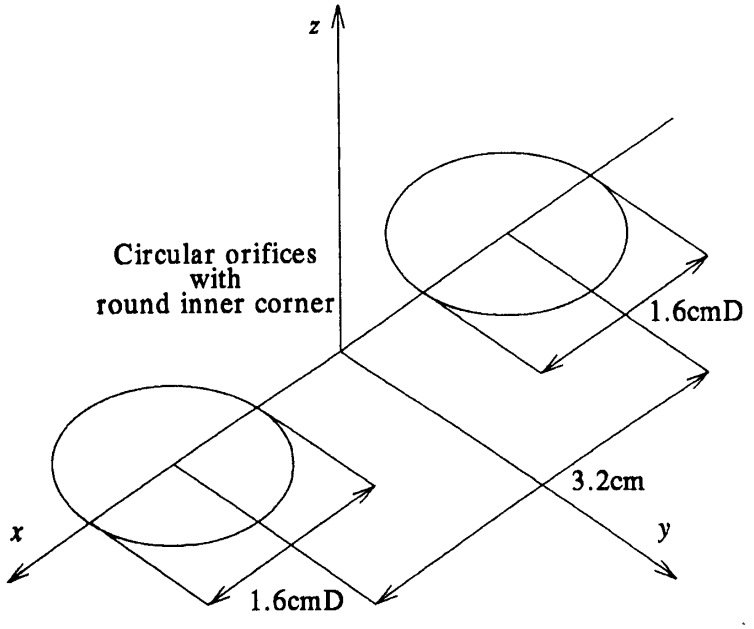

Fig.4 Orifice configuration; two coplanar circular orifices with radius R_o $=0.8$cm are disposed apart their center with $D_o=4R_o$.

ensemble-averaged. After the total of $8\times 16=128$ measurements were carried out at each position in space, the probe moves to the next measuring position. From the 16 ensemble-averaged hot wire response signals the Fourier coefficients were calculated and the three velocity components were determined so as not to include any inconsistency among the solutions at neighboring space positions. The measurement was carried out only in the region of the primary quadrant, that is, $x\geq 0$ and $y\geq 0$.

2.2 Data processing

After all the velocity fields were obtained as a function of time, a data enhancing technique was adopted to intensify the data resolution before the vorticity fields were computed. The velocity components, v_x, v_y and v_z, are given in the measurement area discretized with I points in the x direction, J points in the y direction and K points in the z direction, considering the sets,

$$\begin{aligned}
&x[0]=0,\ x[1]=\Delta x,\ \cdots,\ x[i]=(i-1)\Delta x,\ \cdots,\ x[I-1]=(I-1)\Delta x,\\
&y[0]=0,\ y[1]=\Delta y,\ \cdots,\ y[j]=(j-1)\Delta y,\ \cdots,\ y[J-1]=(J-1)\Delta y,\\
&z[0]=z_o,\ z[1]=z_o+\Delta z,\ \cdots,\ z[k]=z_o+(k-1)\Delta z,\ \cdots,\ z[K-1]=z_o+(K-1)\Delta z,
\end{aligned}$$

where, Δx, Δy and Δz are the spacings of discretization ; z_o is the starting height of the measurement. The measured velocity components are expressed by $v_x[i, j, k]$, $v_y[i, j, k]$ and $v_z[i, j, k]$ at each discretized position $[i, j, k]$, that is, at $x=x[i]$, $y=y[j]$, $z=z[k]$. The simple and effective data enhancement was done by tri-linear interpolation so as not to spoil the substance of the flow field. In this experiment, the following formula was applied over all the measured velocity data ;

$$\begin{aligned}
v_q[i+\delta i, j+\delta j, k+\delta k]=&\\
&\sum_{\alpha=0}^{1}\sum_{\beta=0}^{1}\sum_{\gamma=0}^{1}\{(1-\alpha)(1-\delta i)+\alpha\delta i\}\{(1-\beta)(1-\delta j)+\beta\delta j\}\\
&\cdot\{(1-\gamma)(1-\delta k)+\gamma\delta k\}v_q[i+\alpha, j+\beta, k+\gamma]\\
\text{for}\quad &\delta i=0, \frac{1}{2}, 1\ ;\ \delta j=0, \frac{1}{2}, 1\ ;\ \delta k=0, \frac{1}{2}, 1\\
\text{and}\quad &q=x, y, z\ ;\ i=1, \cdots, I-1\ ;\ j=1, \cdots, J-1\ ;\ k=1, \cdots, K-1. \qquad (2)
\end{aligned}$$

From now, the number of mesh points I, J and K are replaced by the number of enhanced mesh points, $2I-1$, $2J-1$ and $2K-1$, respectively. Spatial filtering on the enhanced velocity field was carried out so as to remove the noise originating independently at each measurement. In this experiment, the following formula, working as a simple low-pass filter, was applied three times over all the velocity data ;

$$\begin{aligned}
&v_q[i, j, k]=\frac{1}{27}\sum_{i'=i-1}^{i+1}\sum_{j'=j-1}^{j+1}\sum_{k'=k-1}^{k+1}v_q[i', j', k']\\
&\text{for}\quad q=x, y, z\ ;\ i=1, \cdots, I\ ;\ j=1, \cdots, J\ ;\ k=1, \cdots, K.
\end{aligned} \qquad (3)$$

The vorticity vector denoted by the boldface symbol $\boldsymbol{\omega}$ can be obtained from the filtered velocity field. Its components ω_x, ω_y and ω_z are defined by

$$\omega_x=\frac{\partial v_z}{\partial y}-\frac{\partial v_y}{\partial z},\quad \omega_y=\frac{\partial v_x}{\partial z}-\frac{\partial v_z}{\partial x},\quad \omega_z=\frac{\partial v_y}{\partial x}-\frac{\partial v_x}{\partial y} \tag{4a,b,c}$$

and are computed in their discretized form as

$$\omega_x[i,j,k]=\frac{v_z[i,j+1,k]-v_z[i,j-1,k]}{2\Delta y}-\frac{v_y[i,j,k+1]-v_y[i,j,k-1]}{2\Delta z}, \tag{5a}$$

$$\omega_y[i,j,k]=\frac{v_x[i,j,k+1]-v_x[i,j,k-1]}{2\Delta z}-\frac{v_z[i+1,j,k]-v_z[i-1,j,k]}{2\Delta x}, \tag{5b}$$

$$\omega_z[i,j,k]=\frac{v_y[i+1,j,k]-v_y[i-1,j,k]}{2\Delta x}-\frac{v_x[i,j+1,k]-v_x[i,j-1,k]}{2\Delta y}. \tag{5c}$$

The vorticity norm is denoted by ω as

$$\omega=\sqrt{{\omega_x}^2+{\omega_y}^2+{\omega_z}^2}. \tag{6}$$

Both the computed velocity and the vorticity data in the primary quadrant were extended to the other three quadrants by using their symmetricalness. That is, each velocity and vorticity components in the neighboring quadrant can be obtained by the following relations:

$$\begin{aligned} &v_x(-x,y,z)=-v_x(x,y,z),\quad v_y(-x,y,z)=v_y(x,y,z),\quad v_z(-x,y,z)=v_z(x,y,z),\\ &\omega_x(-x,y,z)=\omega_x(x,y,z),\quad \omega_y(-x,y,z)=-\omega_y(x,y,z),\quad \omega_z(-x,y,z)=-\omega_z(x,y,z), \end{aligned} \tag{7a}$$

$$\begin{aligned} &v_x(x,-y,z)=v_x(x,y,z),\quad v_y(x,-y,z)=-v_y(x,y,z),\quad v_z(x,-y,z)=v_z(x,y,z),\\ &\omega_x(x,-y,z)=-\omega_x(x,y,z),\quad \omega_y(x,-y,z)=\omega_y(x,y,z),\quad \omega_z(x,-y,z)=-\omega_z(x,y,z). \end{aligned} \tag{7b}$$

2.3 Experimental condition

The condition for the generation of the vortex rings carried out in the present study is given in Table 1. The controllable parameters are the amplitude and duration of the voltage pulse applied to the loudspeaker. First of all, the

Table 1. Condition for vortex generation

case	voltage (V)	duration (ms)	reference velocity $V_{o,MAX}$ (cm/s)	reference Reynolds number $Re_o=\frac{V_{o,MAX}R_o}{\nu}$
C	5	4	532	2890

velocity at the center of the orifice was measured. The axial velocity v_z at the center of the orifice, that is at $x=D_o/2=2R_o=1.6$cm, $y=0$, $z=0$, which is symbolized by V_o, is plotted in Fig. 5. The velocity V_o becomes the maximum value 5.32m/s at $t=4.8$ms. This maximum value of V_o was chosen as the reference velocity which is denoted by $V_{o,MAX}$, where, the subscript '$_{MAX}$' means the maximum value with respect to time. In the present investigation, R_o, the orifice radius, and $V_{o,MAX}$, the maximum velocity at the center of the orifice, were selected to define the reference Reynolds number Re_o, as

$$Re_o=\frac{V_{o,MAX}R_o}{\nu}, \tag{8}$$

where, ν indicates the kinematic viscosity of the fluid (air), and Re_o was 2890 in the present measurement.

The measurement condition is summarized in Table 2, in which the measured region, the grid size, the number of the grid points and those of the enhanced data are given. From the specified time range and the specified time interval Δt, a set of the time discretization used is derived

$$t[0]=t_o,\ t[0]=t_o+\Delta t,\ \cdots,\ t[l]=t_o+(l-1)\Delta t,\ \cdots,\ t[L-1]=t_o+(L-1)\Delta t,$$

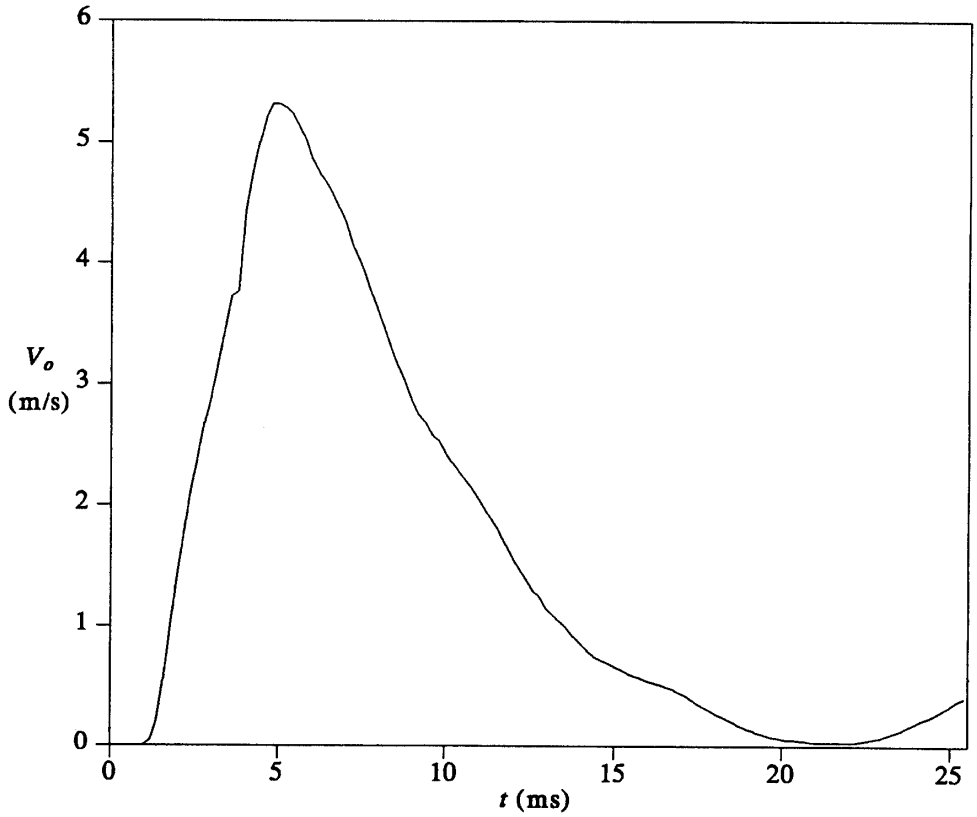

Fig.5 V_o, the axial velocity at the center of the orifice ($x/R_o=2$, $y=0$, $z=0$) versus time.

where, L denotes the number of time grid points and t_o shows the starting time of A/D conversion, which was 0 in the present measurement. It took 85 seconds to obtain a set of 16 ensemble-averaged hot wire responses, which consists of 128 independent signal data, at a fixed point in space, so that 382 hours were expended for this measurement.

The maximum velocity norm v_{max} and the maximum vorticity norm ω_{max} at each instant are plotted in Fig. 6, where, the subscript '$_{max}$' means the maximum value in space at that instant. These values are used to normalize the data at each instant hereafter. The maximum vorticity norm decreases as the time increases, however the maximum velocity norm rises and falls, because the vorticity is a sort of relative value while the velocity field directly presents the interacting vortex rings.

Table 2. Measurement condition

case	space range		spacing	# of grid points		time range	interval	# of time points
	x, y (cm)	z (cm)	$\Delta x, \Delta y, \Delta z$ (cm)	I, J	K	t (ms)	Δt (ms)	L
C (measured)	0.000~3.825	0.300~11.325	0.225	18	50	0.0~91.6	0.4	230
C (enhanced)	0.000~3.825	0.300~11.325	0.1125	35	99	0.0~91.6	0.4	230

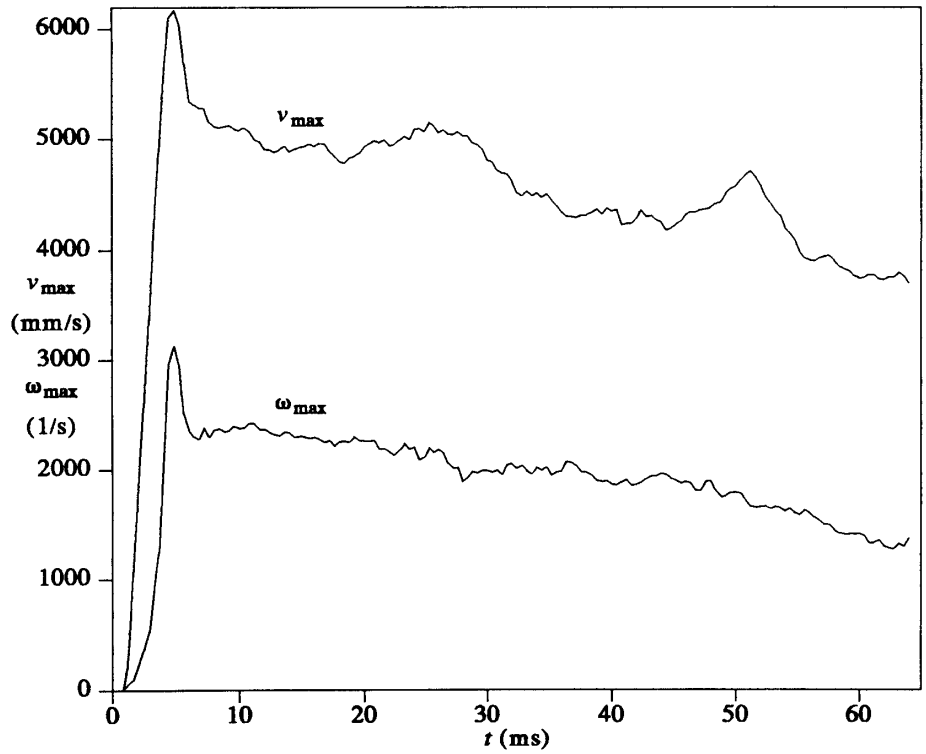

Fig.6 Maximum velocity v_{max} and maximum vorticity ω_{max} versus time, which are used for the normalization.

3. Results And Discussion

3.1 Features on the planes of symmetry

The present phenomenon has two planes of symmetry, $y=0$ and $x=0$, which mean the $x-y$ and $y-z$ planes, respectively. The results on these planes are explained in this section. Figure 7 is the plots of the vorticity contour lines.

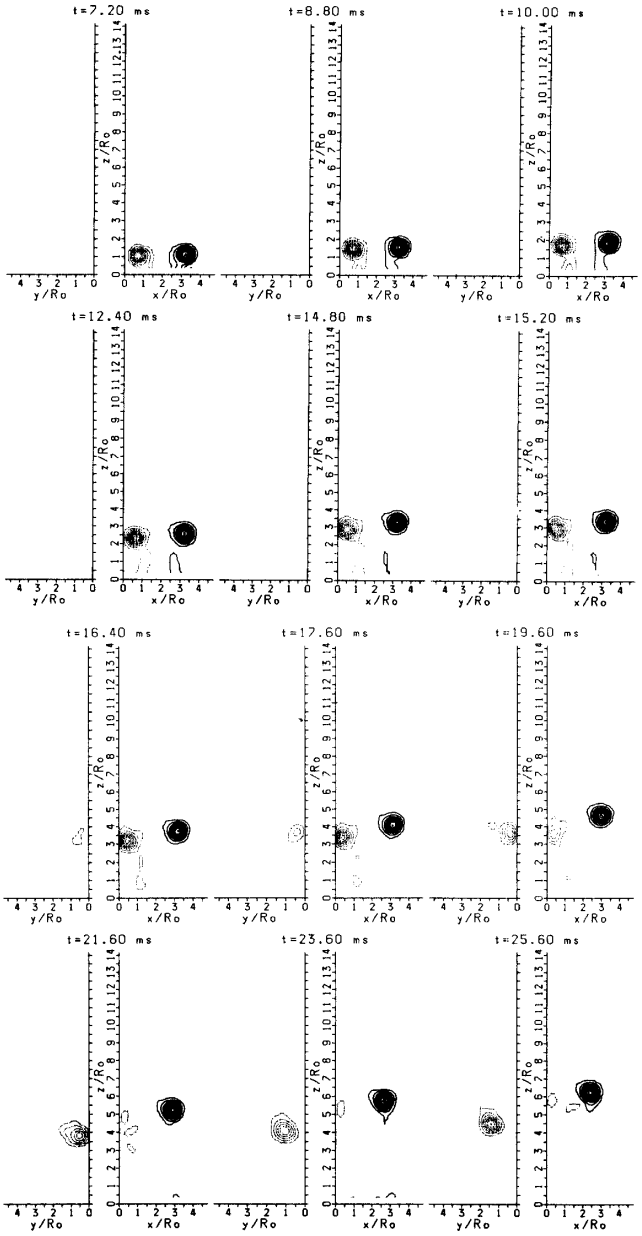

Fig.7 Evolution of the vorticity contour map on the planes of symmetry, $y=0$ on the right side and $x=0$ on the left; the vorticity on these planes has one non-zero component, ω_y and ω_x, respectively, contour lines with clockwise (positive) vorticity are indicated by solid lines and those of counter-clockwise (negative) by dotted lines, and the vorticity is normalized by ω_{max}, the maximum vorticity norm at that instant; the levels of the contour lines are ± 0.0625, ± 0.1875, ± 0.3125, ± 0.4375, ± 0.5625, ± 0.6875, ± 0.8125, ± 0.9375.

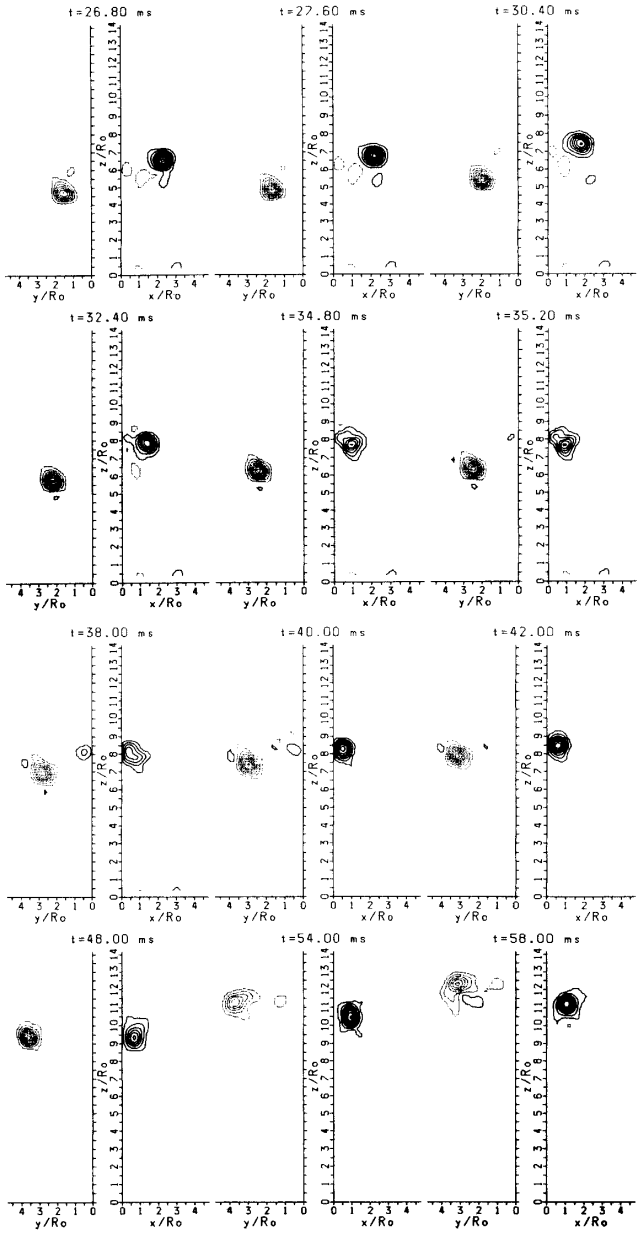

Fig.7 (Continued)

Since the vorticity becomes scalar on these planes of symmetry, ω_y on the plane $y=0$ and ω_x on the plane $x=0$ are to be drawn in the right and left parts on each plot, respectively. The coordinates are normalized by the orifice radius R_o so that the segment from x/R_o through 3 corresponds to the orifice cross-section. The contour lines with positive or clockwise vorticity are indicated by solid lines and those of negative or counter-clockwise vorticity by dotted lines. Both the vorticities, ω_y and ω_x, are normalized by the maximum vorticity norm at that instant ω_{max}, and the interval between each contour line is 0.125 of the maximum vorticity norm. The vorticity is generated along the edge of the orifice and it is assembled to form a transitional vortex ring. The accumulated vorticity is shed at about $t=5$ms to begin to propagate, while the 'trail' vorticity still

connects the primary vortex ring with the orifice edge. Although a vortex ring consists of the 'core', the encircling 'outer ring' and the 'trail' parts, the 'trail' part must be regarded separately from the primary vortex ring. Since the formation process of the vortex ring is almost completed by $t=7.2$ms, we consider this instant as the standard point for the initial property. At this instant, two cross-sections of the ring are detected on the vorticity contour plot. The outside part, denoted by the solid lines in this case whose center is located at $x/R_o=3.16$ and $z/R_o=1.09$, is named as the original 'far' section and the inside part, denoted by the dotted lines in the plot whose center is located at $x/R_o=0.84$ and $z/R_o=1.00$ at that moment, is named as the original 'near' section. The initial radius of the vortex ring is calculated to be $R=1.16R_o$.

Although the self-induced velocity makes the vortex ring move exactly perpendicular to the orifice plane, the mutual-induced velocities between the close segments prevent them from moving up with the same velocity as that of the far section. As a result the near sections go up slowest of the entire ring, therefore the ascending courses of the rings are shifted inward so as to approach each other. The state considered as the moment just before adjoining the near sections is shown at t=10 ms in Fig. 7, in which the center of the near section is located at $x/R_o=0.75$ and $z/R_o=1.73$, when the center of the far one is at $x/R_o=3.20$ and $z/R_o=1.89$. It signifies that the final approaching angle can be taken as 3.7°. The trail vorticity is elongated and either is gradually entrained into the primary vortex ring or decays itself. And the vortex rings are to be fully developed, however the uniting occurs before it.

The mutually induced velocities between the vortex rings make the approaching angle larger and the nearest segments of the rings are adjoined pressing hard against each other. Immediately after the approaching angle reaches 8.7° at $t=$ 14.8ms, a new negative vorticity region appears on the $y-z$ plane at $t=15.2$ms. It is important that its location, $y/R_o=0.55$ and $z/R_o=3.22$, is not on the center line. It is clearly displayed that the new negative vorticity region, which is called the 'cross-linked' vortex tube, becomes larger and larger while the original negative section of the ring on the $x-z$ plane, that is the original near section, becomes smaller and smaller. This cross-linked section corresponds to the 'far' one on the $y-z$ plane.

The near section on the $x-z$ plane is weakened quickly until the time $t=21.6$ms and the near blob is crushed to split into three blobs, while the cross-linked blob grows up to come in touch to the other cross-linked 'far' segment in $y<0$. Immediately after the crushing of the original near blobs, the cross-linked blobs begin to spread out and the split original near blobs stop decaying. Although the original far blob decreases its x-position throughout the approaching, adjoining and cross-linking processes, its z-position is located a long way up from that of the near section. It means that the moving direction of the original far section is inclined up to 25°, which corresponds to the approaching angle, and the united vortex ring makes a saddle shape. As a result a secondary vorticity region appears near the original far blob as shown at $t=$

25.689 in Fig.7 and moreover the original far blob drops its small fragment behind as shown at $t=26.8$ and 27.6ms. As the original far blob approaches the center line, the z-axis, both the wreck of the original near blob and the induced secondary blob decay to disappear by the time $t=34.8$ms. At this instant the unlinking of the original ring can be said to be successfully accomplished. This is the explanation of the first cross-linking between the two vortex rings and unlinking of the original near parts.

From this instant the next step, the second cross-linking begins, but it cannot be accomplished. The original far blobs approaching toward the center line contact each other at $t=34.8$ms and the locally induced velocity makes the adjoining parts pressed each other but not so hard. At the next moment another new positive vorticity area appears around $y/R_o=0.45$ and $z/R_o=8.06$ at $t=35.2$ms. This cross-linked blob does not easily expand out and it begins to shrink after $t=38$ms. On the other hand, the cross-linked far section on the $y-z$ plane goes up and outward by its local induced velocity, accompanying a positive induced secondary vortex blob outside due to the inclination of its moving direction up to 30°. At $t=42$ms the second cross-linked 'near' blob disappears but the original far blob is still touching the other. The induced secondary blob outside the cross-linked far section on the $y-z$ plane decreases as the united vortex ring is level with the orifice plane as shown at $t=48$ms in Fig. 7, when only the united vortex ring exists and no secondary vortices are recognized. From this instant the original far sections begin to spread out separately again because the direction of locally induced velocity is shifted from inward to outward so that the pressing force is extinct. The cross-linked far section on $y-z$ plane goes ahead of the original far blob. It moves inward again due to its continuous large locally induced velocity and follows another induced secondary vortex blob inside the cross-linked far blob as shown at $t=54$ and 58ms in Fig. 7. In this way the second cross-linking stops unsuccessfully.

It is thought that both the instant of starting the cross-linking and that of finishing the unlinking depends on the vorticity level observed on each plane of symmetry. In the extreme case, the observed level of vorticity can be taken as the value small enough to appear in the $y-z$ plane at the very beginning. In other words, the boundaries for the original near sections with much smaller vorticity contact each other as soon as they are generated through the orifices. Thus the definition for cross-linking and unlinking defined to describe this phenomenon. That is, it is necessary to decide which boundaries of the rings are to be observed for the description of this phenomenon.

Figure 8 shows the changes of the positive and negative peaks of the vorticity on each plane of symmetry. The symbols $(\omega_y^+)_{max}$ and $(-\omega_y^-)_{max}$ are almost equivalent to the positive peak vorticity of the original far section on the $x-z$ plane and the negative peak vorticity of the original near section, respectively, and the symbols $(\omega_x^+)_{max}$ and $(-\omega_x^-)_{max}$ are almost equivalent to the positive peak vorticity of the cross-linked near section on the $y-z$ plane and the negative peak vorticity of the cross-linked far section, respectively. The reason for the

usage of 'almost' above is that $(-\omega_y^-)_{max}$ and $(\omega_x^+)_{max}$ do not always exist in the near sections and can be taken by the peaks in the secondary vortices. The value of $(-\omega_x^-)_{max}$ quickly increases during the first cross-linking process and $(-\omega_y^-)_{max}$ rapidly decreases during the first unlinking process. On the other hand, $(\omega_x^+)_{max}$ increases during the second cross-linking process around $t=38$ ms. It is to be noted that the maximum value of the peaks on the planes of symmetry is not equal to the maximum vorticity norm ω_{max}. As presented in Fig. 8, both the cross-linked vorticity peaks $(-\omega_x^-)_{max}$ and $(\omega_x^+)_{max}$ are not zero before $t=14.8$ms, and besides the vorticity peak $(-\omega_y^-)_{max}$ never reaches zero after the unlinking. The reason originates in the spatial continuity of vorticity and in the fluctuation on the measurement.

Since the vortex ring consists of the core region and the surrounding outer ring, it is natural for the description of the cross-linking and unlinking to observe the behavior of the core region, which is defined by the ridgeline of the circumferential velocity around the core center in the local polar coordinates. This core definition is not useful for the transforming or interacting vortex rings because the local velocity field is deformed. Considering the vorticity distribution, the core boundary drawn by the ridgeline is almost equivalent to that drawn by the vorticity level of $0.25\omega_{max}$ (Izutsu & Oshima 1990). It is also known from their results that the mean core radius was $0.23\sim0.42R_o$ and the ring radius was $1.07\sim1.26R_o$ depending on the Reynolds number.

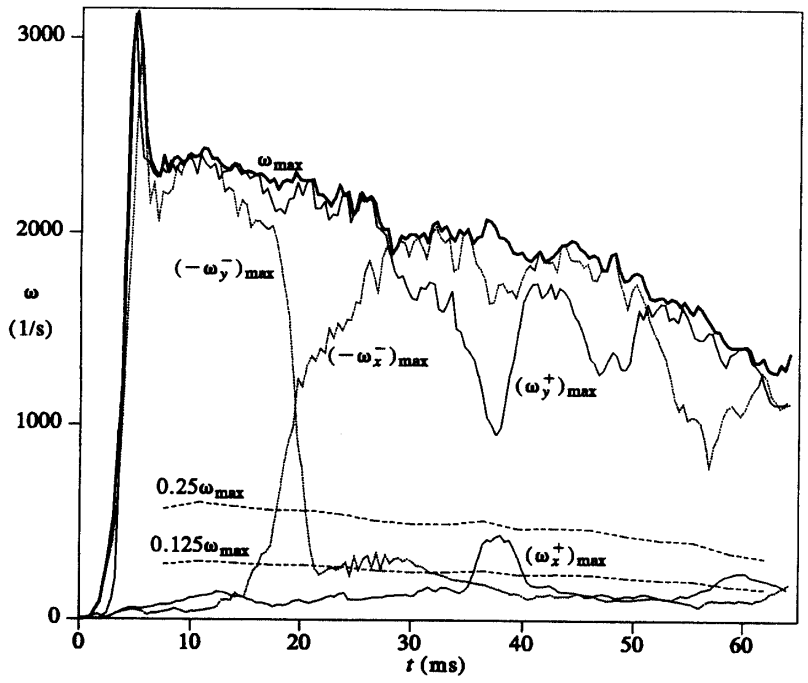

Fig.8 Peak vorticity on each plane of symmetry ; maximum vorticities $(\omega_y^+)_{max}$ and $(-\omega_y^-)_{max}$ on the $x-z$ plane, maximum vorticities $(\omega_x^+)_{max}$ and $(-\omega_x^-)_{max}$ on the $y-z$ plane, maximum vorticity norm at each instant ω_{max} are plotted ; $(\omega_y^+)_{max}$ and $(-\omega_x^-)_{max}$ correspond to the maximum vorticities in the original far and in the cross-linked far sections, respectively.

A free laminar circular vortex ring has an almost Gaussian distribution of the vorticity field written by

$$\omega(r)=\omega_{max}\exp(-r^2), \tag{9}$$

where r is the distance from the core center and the core radius indicated by σ is supposed to satisfy the relation $\omega[r=\sigma]=0.25\omega_{max}$, then $\sigma=\sqrt{\ln 4}$ is obtained from Eq. (9). The circulation along the circle with the radius r_o, which means the specified outer ring radius, is given by

$$\Gamma(r_o)=2\pi\int_0^{r_o}\omega(r)rdr=\pi\{\omega_{max}-\omega(r_o)\}, \tag{10}$$

in particular, the limit circulation is obtained by letting $r_o=\infty$ as

$$\Gamma(\infty)=\pi\,\omega_{max}, \tag{11}$$

thus some evaluation for the relation between the outer ring radius r_o and the circulation $\Gamma(r_o)$ was done in Table 3. As the core radius σ and the vortex ring radius R are assumed by the largest evaluation $0.42R_o$ and $1.26R_o$, respectively, the distance from the axis of the vortex ring to the farthest outer ring side $R+r_o$ is estimated as the value less than $\{0.42(r_o/\sigma)+1.26\}R_o$. For the purpose of investigating the cross-linking and unlinking process, the outer ring boundary must be selected so as not to contact the center line, the z-axis, during the initial stage, thus the relation

$$0.42(r_o/\sigma)+1.26<2, \tag{12}$$

must be satisfied with enough allowance. From the evaluation of the allowance in Eq. (12) as written in Table 3 the proper value $r_o=\sqrt{2}\sigma$ was selected to specify the outer ring radius for the observation of the approaching and cross-linking processes, that is, the vorticity level on the outer ring boundary is to be 0.0625

Table 3. Evaluation of outer ring radius in Gaussian vorticity distribution of circular vortex ring.

outer ring radius r_o/σ	lowest vorticity $\omega[r=r_o]/\omega_{max}$	circulation $\Gamma(r_o)/\Gamma(\infty)$	allowance of Eq.(12) $2-\{0.42(r_o/\sigma)+1.26\}$
1	0.25	0.75	0.32
$\sqrt{1.5}$	0.125	0.875	0.23
$\sqrt{2}$	0.0625	0.9375	0.15
$\sqrt{2.5}$	0.03125	0.96875	0.08
$\sqrt{3}$	0.015625	0.984375	0.01

of the maximum.

In consideration of Fig. 8, the level $0.0627\omega_{max}$ satisfactorily eliminates the small vorticity existing before $t=14.8$ms. It is also known that the core level $0.25\omega_{max}$ hides the second cross-linking process around $t=38$ms, however the middle level $0.125\omega_{max}$ does not. It must be said here that the level $0.25\omega_{max}$ do not always give the true boundary of the core region because of stretching of the vortex tubes, which is discussed in the next section. Comparing the peak vorticity changes on the planes of symmetry in Fig. 8 with the maximum vorticity norm ω_{max} plotted in Fig. 6, which is re-plotted in Fig. 8 by the thick line, the position of the maximum vorticity almost exists on either the $x-z$ plane or the $y-z$ plane. A significant exception happens during the second cross-linking, when the maximum vorticity norm is placed out of both the planes of symmetry and the peak vorticity $(\omega_y^+)_{max}$ in the original far section falls in on a large scale. Moreover, it declines again around $t=48$ms, while the peak vorticity $(-\omega_x^-)_{max}$ in the cross-linked far section falls in from $t=50$ to 62ms.

The most fundamental approach to describe the uniting process, which consists of the first cross-linking and unlinking, the second cross-linking and the decay, is to observe the change of the circulation denoted by the summation of vorticity. Moreover the circulation is the only quantitative measure for describing the progress rate of the cross-linking and unlinking. It is however meaningless for the description of this uniting process to sum up the entire vorticity on each plane of symmetry, that is, to get $\Gamma(\infty)$ on the plane. By determining the integral boundary, that is the outer ring radius r_o, as $\sqrt{2}\sigma$, in other words, by totaling the vorticity greater than $0.0625\omega_{max}$ on each plane of symmetry, the process is clearly described on the plot of four characteristic circulations as shown in Fig. 9. The original far and near circulations,

$$\Gamma_y^+=\int\omega_y(x, y=0, z)dxdz \quad \text{for} \quad \omega_y\geq 0.0625\omega_{max} \quad \text{without trail,} \tag{13a}$$

$$\Gamma_y^-=\int\omega_y(x, y=0, z)dxdz \quad \text{for} \quad \omega_y\leq -0.0625\omega_{max} \quad \text{without trail,} \tag{13b}$$

and the cross-linked far and near circulations,

$$\Gamma_x^-=\int\omega_x(x=0, y, z)dydz \quad \text{for} \quad \omega_x\leq -0.0625\,\omega_{max}, \tag{13c}$$

$$\Gamma_x^+=\int\omega_x(x=0, y, z)dydz \quad \text{for} \quad \omega_x\geq 0.0625\,\omega_{max}, \tag{13d}$$

are defined on each plane of symmetry. These circulations exclude the trail vorticity. The trail circulation is separately computed on the far section,

$$\Gamma_{y,t}^+=\int\omega_y(x, y=0, z)dxdz \quad \text{for} \quad \omega_x\geq 0.0625\omega_{max} \quad \text{within trail,} \tag{14a}$$

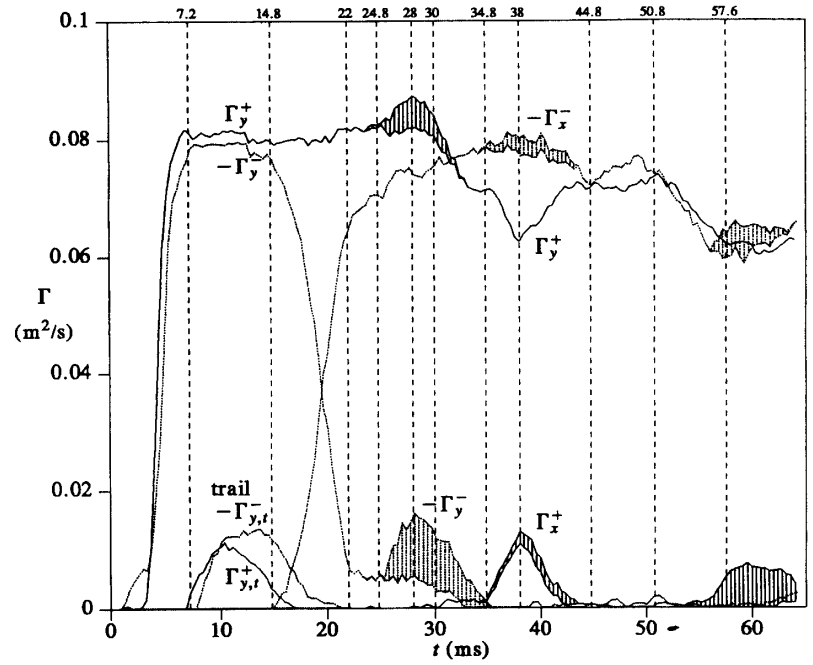

Fig.9(a) Circulations of 93.75% of the original far and near sections, and of the cross-linked far and near sections, Γ_y^+, $-\Gamma_y^-$, $-\Gamma_x^-$, Γ_x^+, respectively; trail circulations are separately plotted with the original far and near sections as $\Gamma_{y,t}^+$ and $-\Gamma_{y,t}^-$, respectively; hatched area shows the circulation of the secondary vortices of which the axis exists on either the $x-z$ or $y-z$ plane.

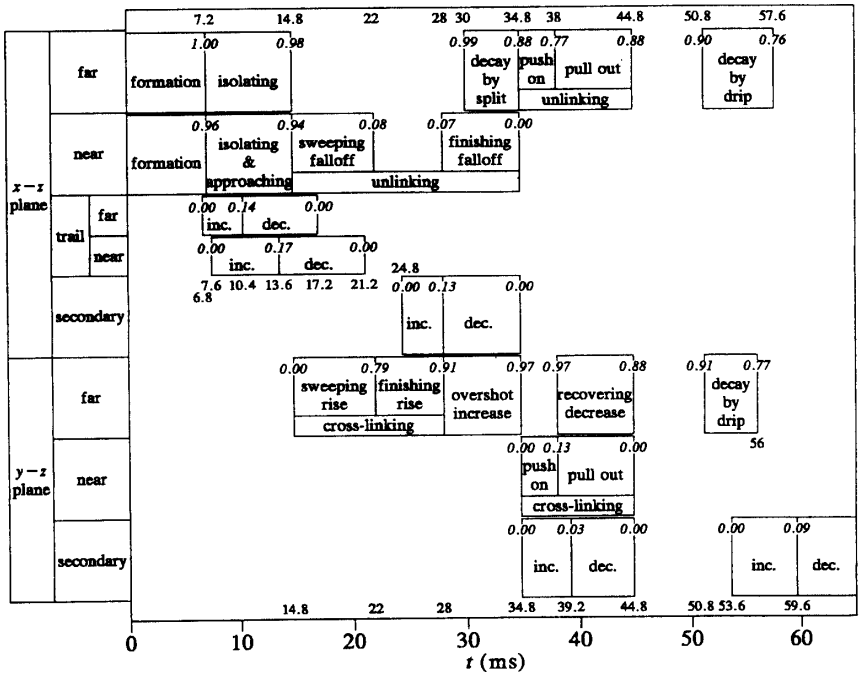

Fig.9(b) Phase chart for the process of the uniting two circular vortex rings; after the decay phase by dripping the united ring behaves like an elliptic vortex ring.

and on the near section,

$$\Gamma_{y,t}^{-}=\int\omega_y(x, y=0, z)dxdz \quad \text{for} \quad \omega_x\leq -0.0625\omega_{max} \text{ within trail,} \tag{14b}$$

by counting only the trail part. Because the vorticity cutoff level is 0.0625, these circulations are named as the 93.75% level circulations. Hereafter the circulation means this 93.75% level circulation. The changes of these characteristic circulations are plotted on Fig. 9(a).

As soon as the two vortex rings begin to be generated, the far segment ascends slightly ahead of the near one due to the mutual induced velocity. Therefore the circulation of the far section Γ_y^+ grows faster than that of the near $-\Gamma_y^-$. It becomes steady at $t=7.2$ms, when the property of the ring is considered as the standard or initial state, and begins to separate clearly into the primary ring and the trail part. The initial circulation Γ_o is supposed to be that of the original far section at $t=7.2$ms. It is 813.2cm^2/s and the circulation of the original near section at that instant is 784.0cm^2/s which corresponds to about $0.98\Gamma_o$. Here, the Reynolds number of the original vortex ring Re can be defined by the initial circulation Γ_o and the kinematic viscosity ν as

$$Re=\frac{\Gamma_o}{\nu}, \tag{15}$$

which is 5520 in the present measurement. Figure 9(b) shows the phase chart explaining the turning points of the circulations on the planes of symmetry interpreted from Fig. 9(a). A Roman figures written in Roman figures shows the time of a turning point and that in italics presents the circulation normalized by the initial circulation Γ_o. By the strong mutual velocities having the near segment press downward, it leaves more trail part than the far does, thus the circulation of the near section becomes smaller than that of the far section, substituting that the near trail circulation becomes larger than the far trail one. Therefore the total circulation of the original far section added by the trail component becomes about $1.14\Gamma_o$ and is approximately equal to that of the near section. The trail circulation gradually decays after splitting from the primary ring. Around $t=12.6$ms in the isolating phase, both the circulations of the original far and near sections slightly changes to be 98.3% of the initial state at $t=7.2$ms. The formation, isolating & approaching phases finish up to $t=14.8$ ms. At this instant the circulation of the original near section $-\Gamma_y^-$ begins to decrease and simultaneously that of the cross-linked far $-\Gamma_x^-$ begins to increase. The unlinking process proceeds until $t=22$ms and then suddenly stops decreasing. This quick decrease in the 'sweeping falloff' phase makes the original near section lose about 92% of the initial circulation. The circulation of the original far section Γ_y^+ never changes during this sweeping phase in the

first cross-linking and unlinking term.

The finishing phase of the first cross-linking and unlinking begins with 'swingback' by increasing the circulations both of the original far and of the original near sections after $t=24.8$ms. They reaches up to 13% of Γ_o. This increase is caused by the appearance of the induced secondary vortex ring underneath the original ring. A induced secondary vortex ring has its axis on the plane of symmetry so that both the circulation of the far section and the near section increase. Therefore these increased circulations can be separately calculated and are plotted by the hatched areas in Fig. 9(a). During the 'overshot increase' phase the circulation of the cross-linked far section gradually increases until $t=34.8$ms, and the secondary vortex ring disappears at this instant. However, during the 'finishing falloff' phase of the unlinking process from $t=30$ through 34.8ms, the original far section loses about 11% of the initial circulation.

From this instant the second cross-linking term begins by increasing the circulation of the cross-linked near section Γ_x^+ and decreasing that of the original far section Γ_y^+ . After the 'push on' phase, they reach the peaks at $t=$ 38ms and then they recover the circulations of $t=34.8$ms during the 'pull out' phase. During this the second cross-linking term, a small secondary vortex ring appears and disappears outside the cross-linked far segment and it increases the circulations of the cross-linked far and near sections about 3% of Γ_o, and then both the circulations Γ_y^+ and $-\Gamma_x^-$ becomes equal at $t=44.8$ms as shown in Fig. 9(a). In this way, the second cross-linking and unlinking progresses at 13% of the initial circulation Γ_o, and the remained circulation at $t=44.8$ms is about 88% of the initial circulation Γ_o.

After a stagnant phase from $t=44.8$ to 50.8ms, both the circulations of the original far and the cross-linked far sections begin to decrease suddenly by about 13% of the initial circulation. Since, no particular changes are recognized on the $y-z$ plane, the decay can be said to progress out of the planes of symmetry. After this 'decay' phase from $t=50.8$ through 57.6ms, the circulation remains only 76% of the initial one, and then another swingback begins by the appearance of another secondary vortex ring inside and below the cross-linked far segment. Its circulation is about 9% of the initial circulation Γ_o. Secondary vortices which appeared in the swingback phases are caused by the inclination of the velocity field due to the large inward or outward velocity of the far segments, so that those phenomena are not concerned with the cross-linking and unlinking.

3.2 Vorticity and vortex tubes

In order to realize the whole shape of the transformation and interaction in the uniting vortex rings, the vector vorticity must be presented in three dimensional space. Since it is useless for the understanding of three dimensional vortex tubes to display the innumerable number of vorticity vectors, some scalar value is necessary for easily understandable displaying. Although almost all researchers

have used the vorticity norm for this purpose and the iso-surfaces of somewhat adequate and groundless level are drawn, the segments with the same vorticity norm cannot always present a connected vorticity region nor a vortex tube.

Figure 10 shows the evolution of such iso-surfaces of the vorticity norm fields in the uniting vortex rings. The surfaces of the levels 0.125, 0.25, 0.5 and 0.75 of the maximum vorticity norm at each instant ω_{max} are drawn with the colors white, yellow, orange and red, respectively. Two circular vortex rings are formed side by side as shown at $t=10$ms in Fig. 10 and are pressed hard against each other in the adjoining part around the z-axis. It is represented by the iso-surfaces of level 0.125 and 0.25 at $t=15.2$ms in Fig. 11, in which the form is drawn within the primary quadrant together with the top, side and front views on the upper right, lower left and lower right plots, respectively. The surface with solid lines indicates the lower value side and that of dotted lines indicates the higher. They begin to be cross-linked at two points in the adjoining region and to unlink in the original near segments. After the cross-linked section appears on the $y-z$ plane, it moves to rather the upper position than the original near segment as indicated at $t=18$ms in Fig. 11. At $t=19.2$ms, the process is half-done and the vorticity with the level 0.75 does not appear in both the cross-linked and unlinked segments and that of 0.5 is not recognized in the cross-linked region. By $t=22$ms the cross-linking and unlinking process is almost completed and the vorticity level 0.125 is also unlinked in the original near regions. However the vorticity level 0.75 is not cross-linked yet. Four projections burst temporarily on the united vortex ring and the cross-linked segments being spread out by their outward locally induced velocities while the original far segments are moving inward to approach each other also by their locally induced velocities. The weakened original near vorticity is again concentrated by vortex stretching to appear the level above of 0.125. It is recognized as the two parallel arciform bridges at $t=28$ms, which is clearly plotted on the figure of $t=28$ms in Fig. 11. It is also known that two secondary vortices exist inside the united ring and that the original far segment drops a vortex tube behind by splitting as already pointed out in Fig. 7. These split vortex tubes are quickly weakened to cause a decrease of the original far circulation during the phase from $t=30$ through 34.8ms. At $t=28$ms the four neutral points among the original far and cross-linked far segments, which have quick transformations by their large locally induced velocities, keep no vorticity level of 0.75. As the cross-linked far segments spread out further, both the stretched original near segments and the secondary vortices become weaken and a distorted vortex ring remains by $t=34.8$ms. However the four wrecked blobs of the original near segments still exist like projections on the ring and are moving to be attracted into the approaching original far segments as shown from $t=30.4$ through 38ms in Fig. 10.

From $t=34.8$ms the original far segments are adjoined each other and the second cross-linking starts. As they are close, the peak vorticity on the original far section decreases to disappear at the vorticity level of 0.75. The state most

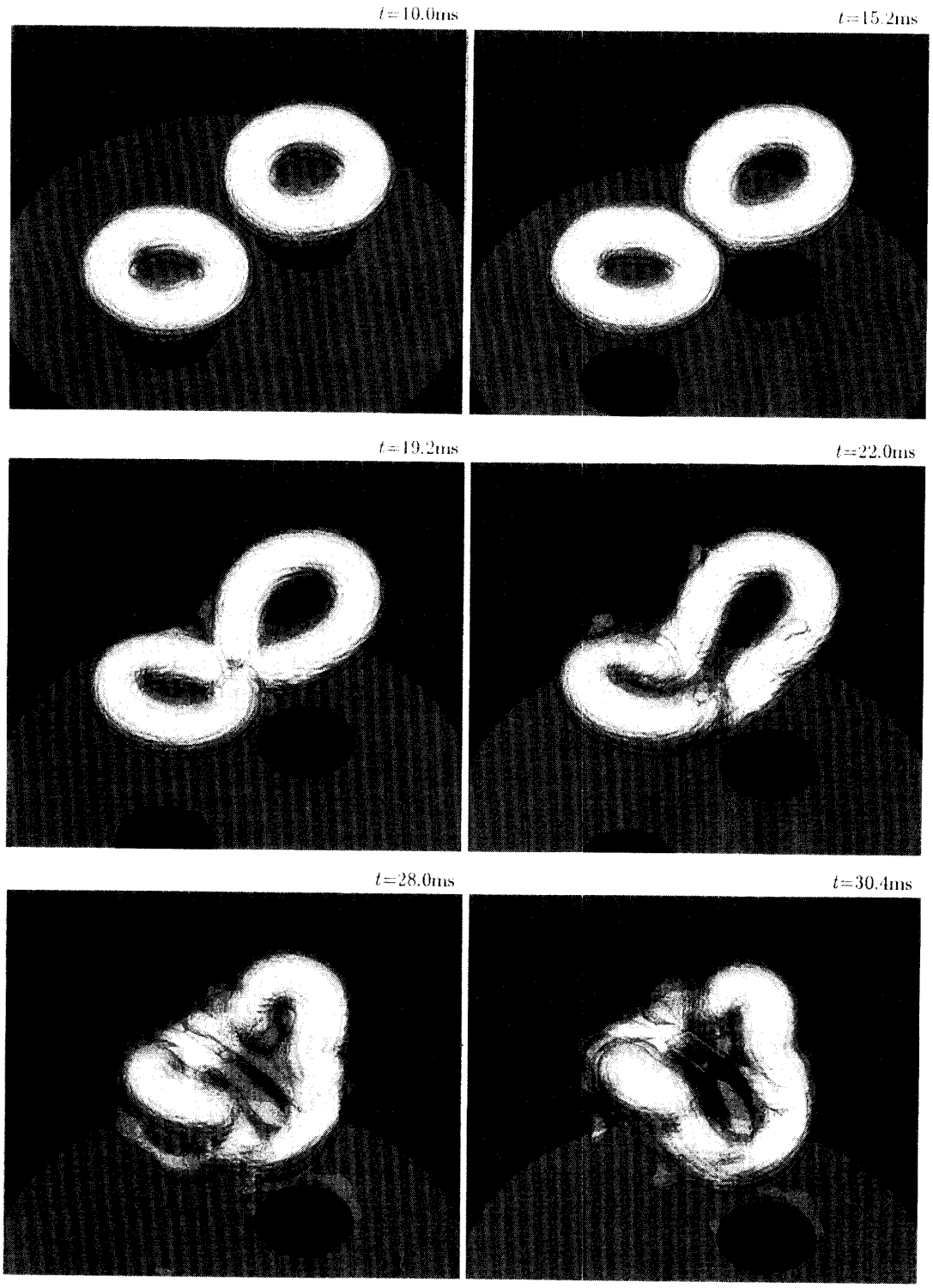

Fig.10 Evolution of the iso-surfaces of the vorticity norm field in the uniting vortex rings; the surfaces of the level 0.125, 0.25, 0.5 and 0.75 of the maximum vorticity norm at each instant ω_{max} are drawn white, yellow, orange and red, respectively.

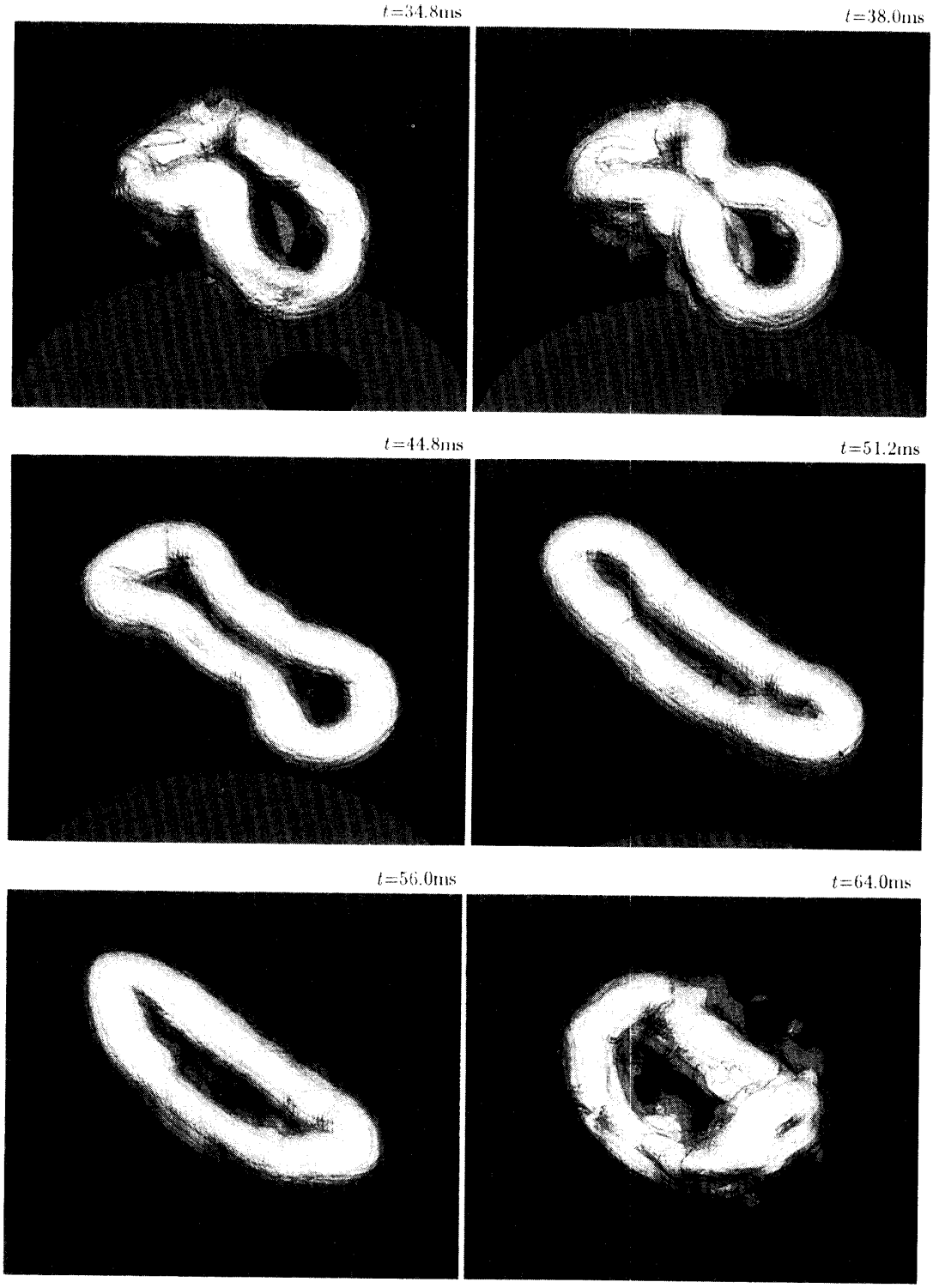

Fig.10 (Continued)

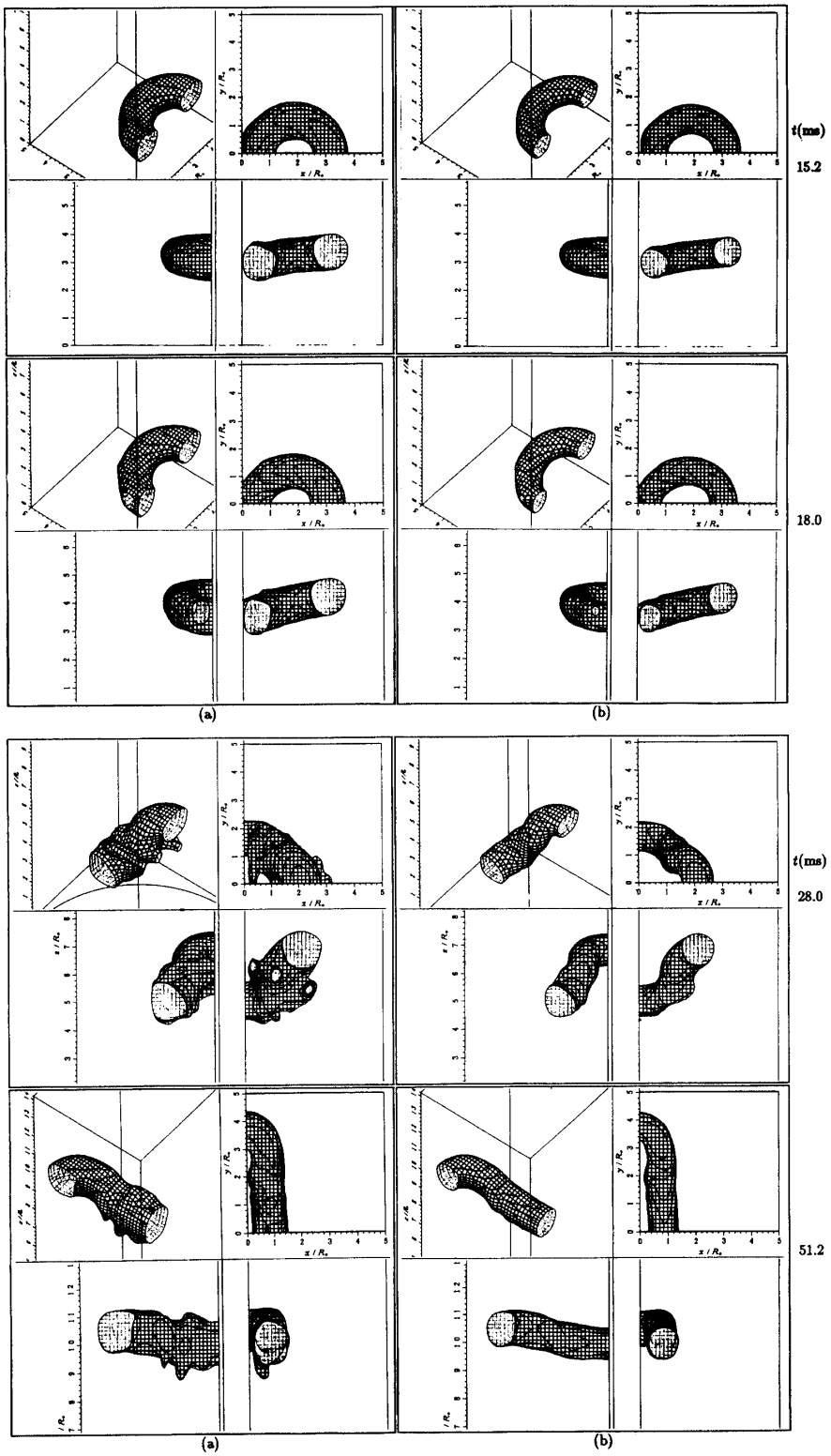

Fig.11 Iso-surfaces of level (a) 0.125 and (b) 0.25 of the maximum are drawn within the primary quadrant together with the top, side and front views on the right upper, left lower and right lower plots, respectively ; the surface with solid lines indicates the lower value side and that of dotted lines indicate the higher.

pushed on is realized at $t=38$ms and the contacting original far segments stop moving up by the balance of the induced velocities acting on them. On the contrary, the cross-linked far segments still spread out more and the situation being almost at a level with the orifice plane comes in around $t=44.8$ms. After the second cross-linking of the united vortex ring stops, it behaves like an elliptic vortex ring with a large aspect ratio. Because of the continued large local induced velocities near the cross-linked far segments they go inward again as shown in the plots from $t=51.2$ through 64ms. From around $t=51.2$ms the 'dripping' of vorticity happens one after another from the wide range of the bottom of the ring as visibly plotted in Fig. 11, therefore the circulation of both the original far and cross-linked near sections quickly decreases in the decay phase.

The second approach to specify the instant of starting the cross-linking and that of finishing the unlinking is the regulation of the maximum vorticity norm ω_{max} by the vorticity level of 0.125 and 0.25. The results are summarized in Table 4, in which the regulation by the circulation, which is already mentioned on Fig. 9(b), is equivalent to that by the vorticity level 0.0625 of the maximum due to the definition of the circulation. By evaluating the time from the beginning of the cross-linking to the completion of the unlinking, it takes 19.8 ms for the first cross-linking and unlinking process and 10ms for the second unsuccessful process on the circulation level. However the vorticity level 0.125 leads to 4.8ms for the first term and 4.4ms for the second, while the vorticity level 0.25 leads to only 2.4ms for the first term.

In order to present the uniting vortex rings, it is better to consider vortex tubes as defined by envelopes surrounding vortex lines. A vortex line can be computed by means of direct integration of the vorticity field based on the definition of the vortex line. The governing equations for the vortex line are

$$\frac{dx}{\omega_x(x, y, z, t)}=\frac{dy}{\omega_y(x, y, z, t)}=\frac{dz}{\omega_z(x, y, z, t)}=ds, \tag{16}$$

where, s is the parameter along each wortex line. Therefore, the simultaneous equations,

$$\frac{dx}{dx}=\omega_x(x, y, z, t),\ \frac{dy}{ds}=\omega_y(x, y, z, t),\ \frac{dz}{ds}=\omega_z(x, y, z, t), \tag{17a,b,c}$$

were numerically integrated starting from the point at which the vorticity norm is greater than the specified lower limit ω_o, on both the $x-z$ and the $y-z$ planes. The time t is treated as a constant and the integral step ds is taken as both a small positive and negative value. Therefore, there can be four starting points for integration in maximum. The integration is continued until the vortex line again crosses the $x-z$ or the $y-z$ plane. Thus a bundle of vorticity lines, including the points within the sections which have the vorticity norm greater

than the specified lower limit ω_o, can be obtained. Next a curved surface surrounding this bundle of vorticity lines is computed to be displayed as an envelope. This is a vortex tube prescribed by the specified lower limit vorticity ω_o.

Figure 12 shows the evolution of the computed envelopes of the vortex lines in the uniting vortex rings. The surfaces of which the specified lower limit level are 0.125, 0.25, 0.5 and 0.75 of the maximum vorticity norm at each instant ω_{max} are drawn colors of white, yellow, orange and red, respectively. Since the integrating path can be swayed in passing over a somewhat fluctuated point in the measured velocity field, consequently the displayed envelope becomes slightly thick depending on the fluctuation of the measurement. Both the vorticity and the vortex tubes begin to cross-link at the same positions apart from the center line, the z-axis. Although the vorticity of the levels 0.5 and 0.75 does not exist in the cross-linked sections, the computed vortex tubes of the levels 0.5 and 0.75 actually does in the cross-linked segments, as shown at $t=19.2$ and 22ms in Figs. 10 and 12. Moreover the display of the vortex tubes at $t=28$ms in Fig. 12 shows that the two arciform bridge vortices linked between the cross-linked segments are in reality two vortex rings which again appear. It is represented by the iso-surfaces of level 0.125 and 0.25 at $t=28$ms in Fig. 13, in which the form is drawn within the primary quadrant together with the top, side and front views on the upper right, lower left and lower right plots, respectively. The surface with solid lines indicates the lower value side and that of dotted lines indicates the higher. The real vortex tube is displayed thicker in the original far segments than in the cross-linked far segments st $t=28$ and 30.4ms, in which the original far segment is moving inward rapidly. The remaining plots of $t=34.8$ through 64ms also prove that even the vortex tube of level 0.75 is always completely connected in a distorted vortex ring. It is known from Fig. 12 that the plot of $t=44.8$ms shows the vorticity bursts under the united vortex ring and that the plot of $t=51.2$ms clearly shows the existence of the two bursts of the vortex tube above the united vortex ring. These situations are not observed in the display of the vorticity norm in Fig. 10. As mentioned above, the interpretation by only using the display of the vorticity norm can possibly lead to the misreading of the phenomenon. The behavior of the vortex tube as well as the vorticity norm, which definitely present the vortex ring, must be pursued to study the interaction of vortex rings.

3.3 First cross-linking and unlinking

In order to know what happens in the region of the first cross-linking and unlinking and how to progress, not the vorticity field but the velocity field must be examined because the vorticity is only the rotation of velocity which characterizes a kind of relative velocity. Figure 14 expresses the evolution of the velocity field of v_z. The contour lines of v_z normalized by the maximum velocity norm v_{max} on both the planes of symmetry are plotted by the dotted lines for positive or upward flow and by the solid lines for negative or downward flow.

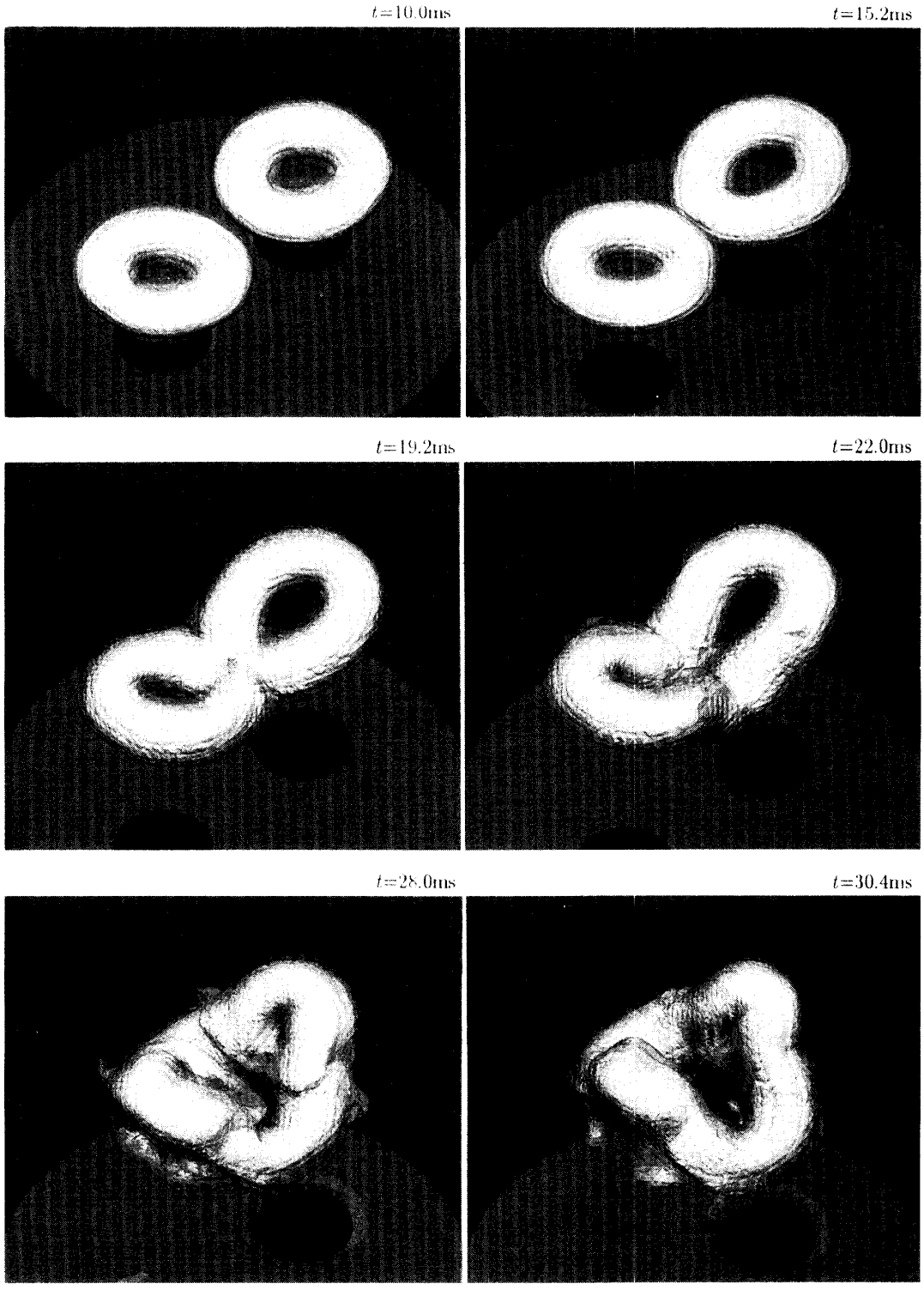

Fig 12 Evolution of the computed envelopes of the vortex lines (vortex tubes) in the uniting vortex rings; the surfaces of which specified lower limit level are 0.125, 0.25, 0.5 and 0.75 of the maximum vorticity norm at each instant ω_{max} are drawn with the colors of white, yellow, orange and red, respectively.

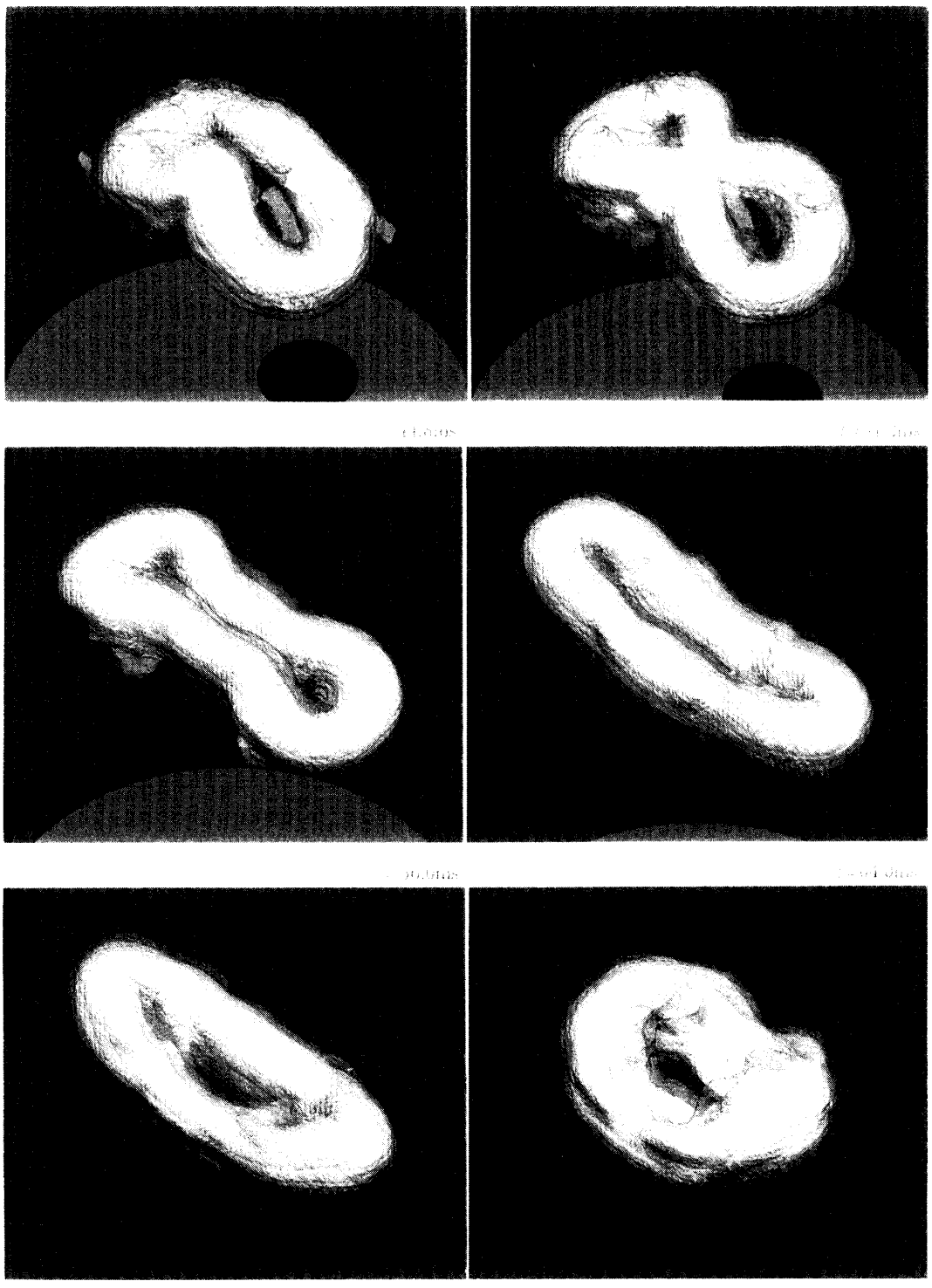

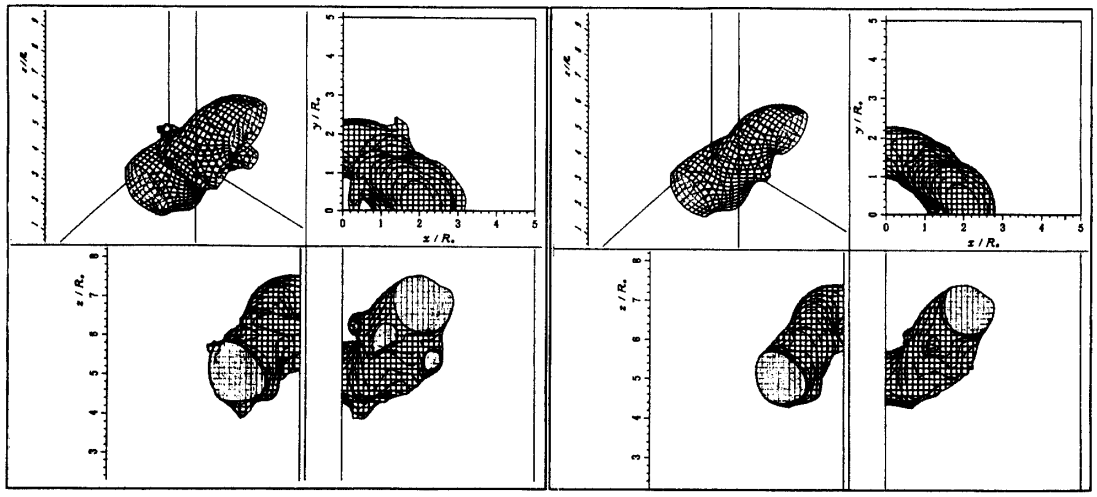

Fig.13 Vortex tubes of the level (a) 0.125 and (b) 0.25 of the maximum are drawn within the primary quadrant together with the top, side and front views on the upper right, lower left and lower right plots, respectively ; the surface with solid lines indicates the lower value side and that of dotted lines does the higher.

That is, the dotted lines show the ascending flow region and the solid ones do the return flow. The interval of each contour line is 0.059 of the maximum vorticity norm. At $t=7.2$ms the cross section of the formed vortex ring can be recognized by the two areas with dense vertical lines due to the definition of vorticity ω_y derived in Eq. (4b). The term of $\partial v_x/\partial z$ is not dominant to the vorticity ω_y in this flow. The curvature of the ring makes the contour lines of v_z even on the $y-z$ plane, however the peak point of return flow is at $x/R_o=0.25$ on the $x-z$ plane. As the original near section approaches the center line, the z-axis, the contour lines near the center line on both the $x-y$ and the $y-z$ planes become dense and the number of them increases rapidly. It means that on the $x-z$ plane the return flow region of the original near section is pressed toward the z-axis to quickly become narrow and restricted so that the speed of the return flow increases radically. The point of the fastest return flow is pushed on to the center line. This is clearly shown by the difference between the plots of $t=7.2$ and 14.8ms in Fig. 14. Moreover, as the returning flow region becomes narrow, it bulges in the positive y direction and the downward flow on the center line is accelerated to become triple the initial state. Immediately after that, the acceleration is temporally slackened and the peak return flow point on the center line is pushed out on the $y-z$ plane by $t=16.4$ms, to be observed in the vorticity field on the $y-z$ plane as a rapid concentration of vorticity. This process is also presented by the top view of Fig. 15 which is the contour map of vertically totaled v_z,

$$\sum_{k=1}^{K} v_z[i, j, k]\Delta z,$$

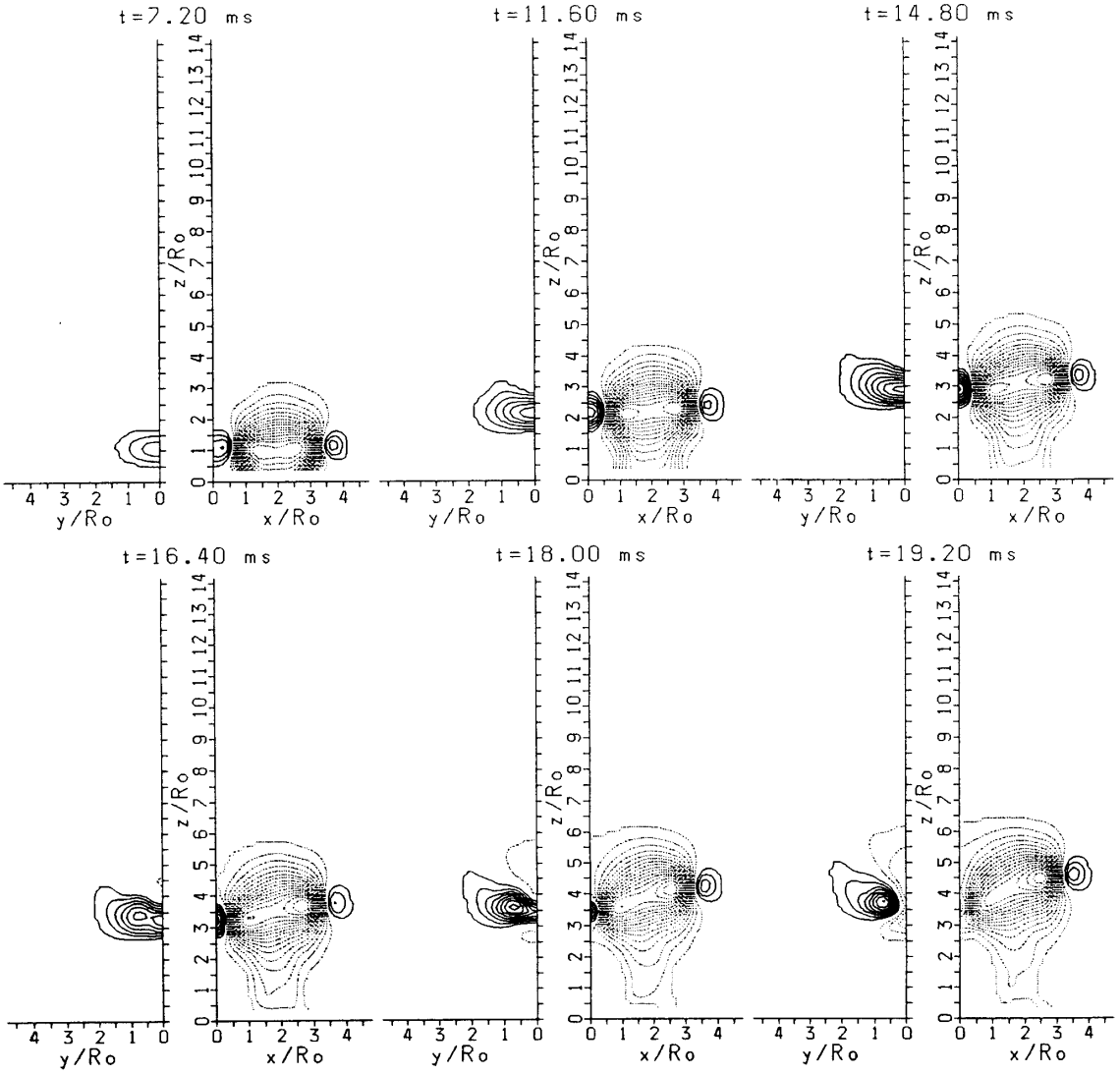

Fig.14 Evolution of velocity contour map of v_z on the planes of symmetry, $y=0$ on the right side and $x=0$ on the left; contour lines with positive (upward) velocity are indicated by dotted lines and those of negative (downward) by solid lines, and the velocity is normalized by v_{max}, the maximum velocity norm at that instant; the levels of the contour lines are ± 0.0625, ± 0.1208, ± 0.1792, $\cdots$, ± 0.9375.

in the unit area on the $x-y$ coordinates. The dotted lines show the positive or upward momentum and the interval of each line is $500\Delta z\text{cm}^2/\text{s}$. The solid lines show the negative or downward momentum and the interval of each line is $100\ \Delta z\text{cm}^2/\text{s}$. The return flow region distributed outside the vortex ring has its high speed area in the gap of the rings due to the limited space of the returning flow region as shown in the plot of $t=7.2$ms in Fig. 15. Since this return flow region is compressed by approaching the original near segments, the same amount of

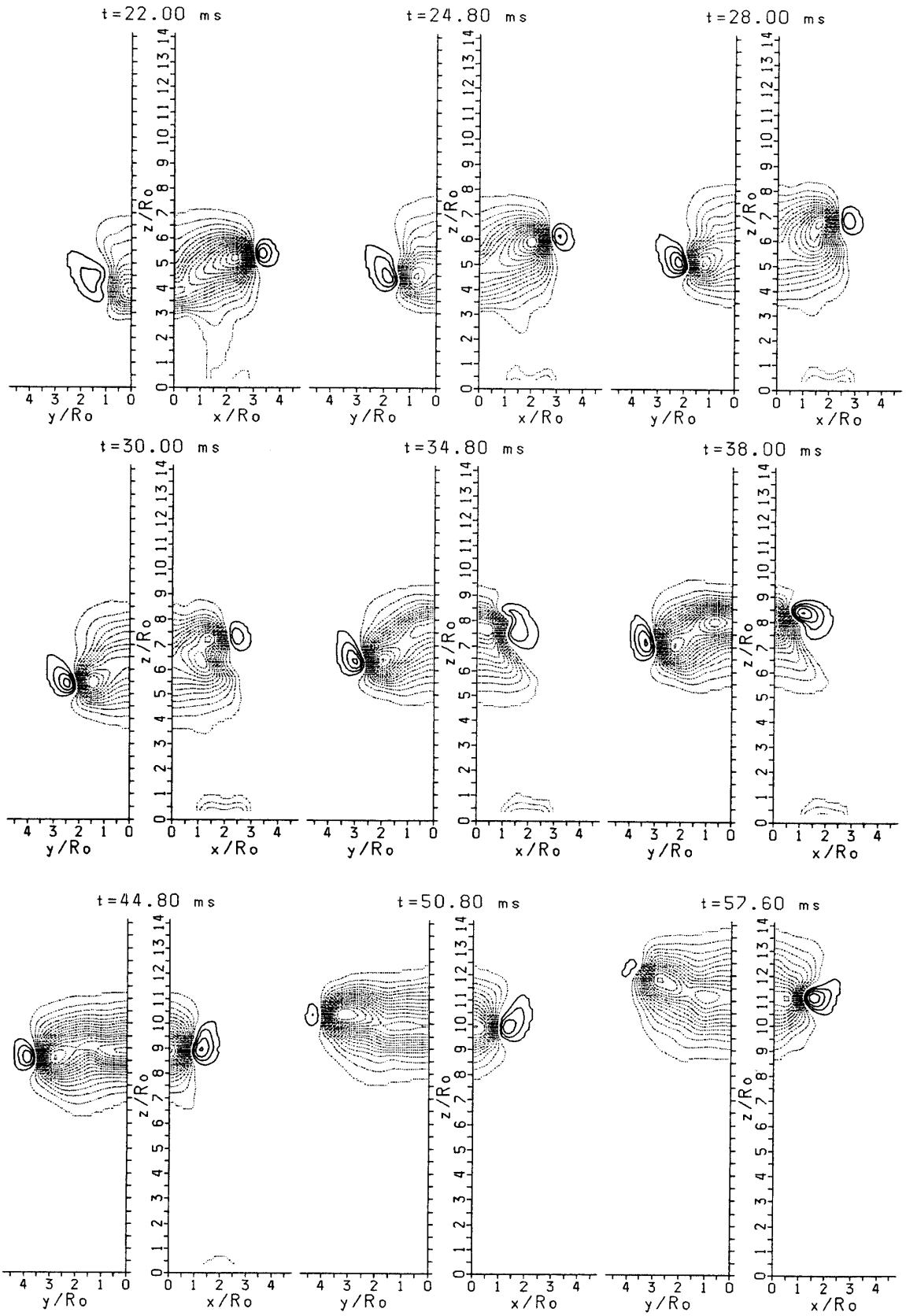

Fig.14 (Continued)

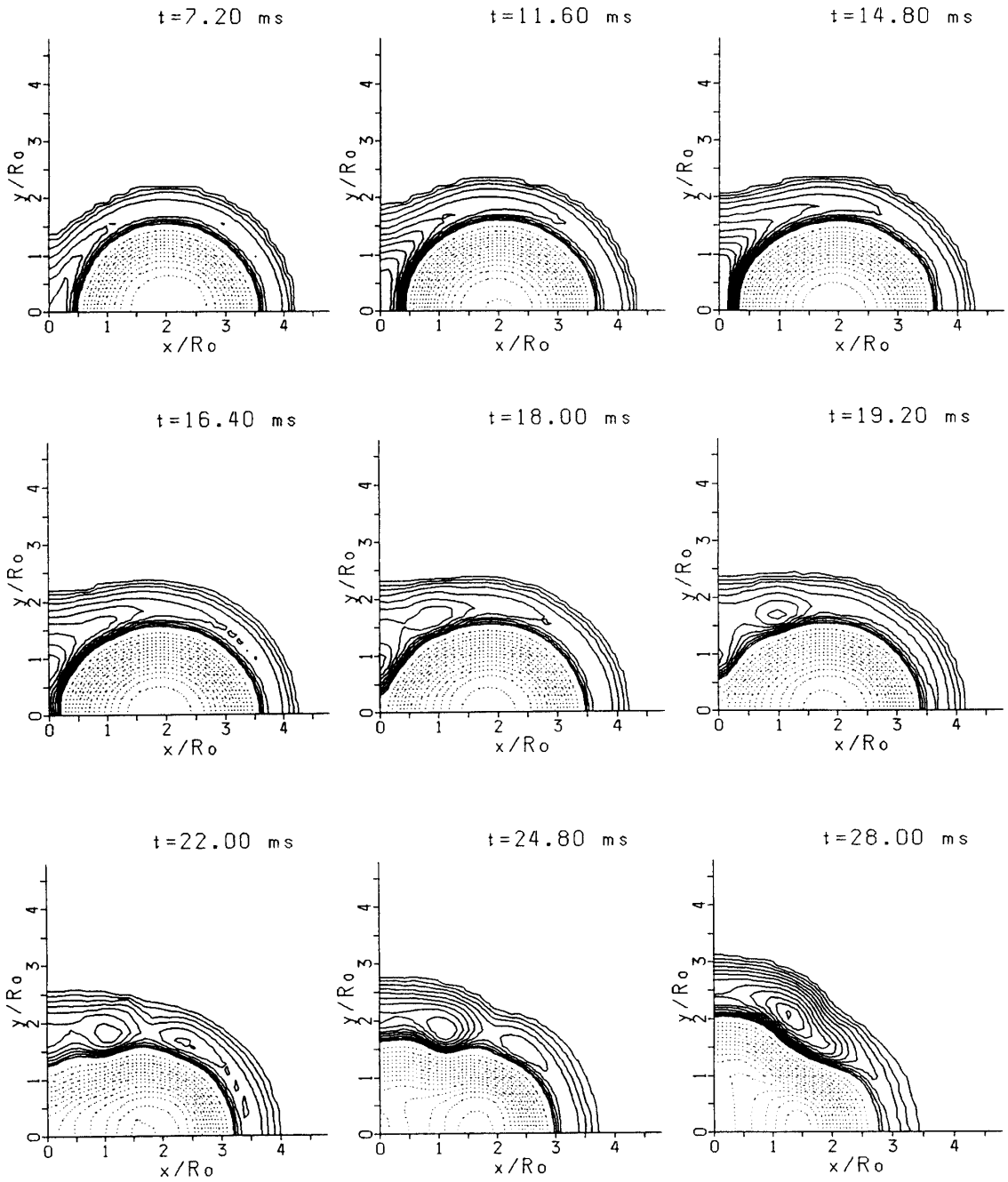

Fig.15 Evolution for contour map of vertically totaled v_z, $\sum_{k=1}^{K} v_z[i, j, k]\Delta z$, on the $x-y$ plane; dotted contour lines indicate the positive (upward) momentum and solid lines do the negative (downward) momentum region, the interval of the contour lines is $500\Delta z \mathrm{cm}^2/\mathrm{s}$ for positive dotted lines and $100\Delta z \mathrm{cm}^2/\mathrm{s}$ for negative solid ones.

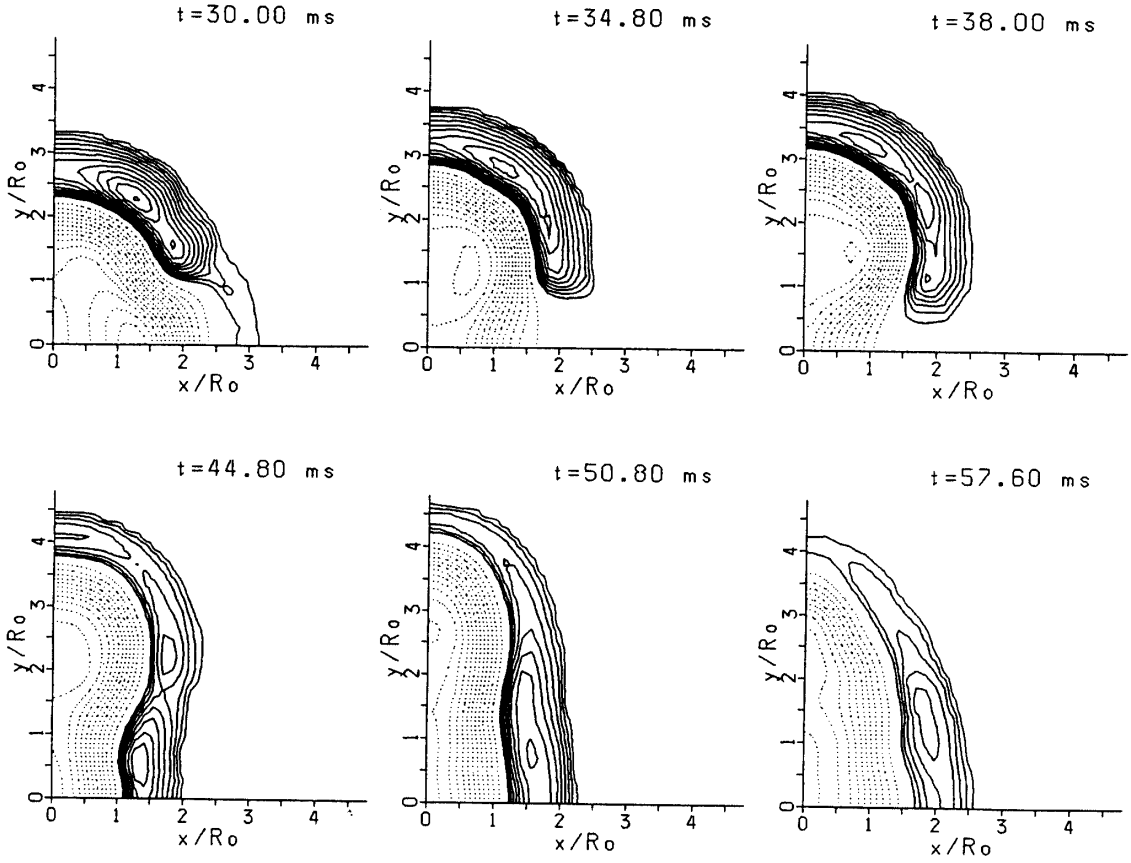

Fig.15 (Continued)

return flux is attained by two means. One is the acceleration of the return flow, and the other is the outward enlargement of the return flow region which is advanced towards both the positive y direction and the far segment along the periphery of the ring. The acceleration of the return flow is proved by the solid line of $(-v_z)_{max}$ plotted in Fig. 16. In this figure, the maximum downward velocity $(-v_z)_{max}$ begins to move from the point on the $x-z$ plane to that on the center line soon after the standard state of t=7.2 ms. It is known that the maximum upward velocity $(v_z)_{max}$ is about triple the maximum downward velocity in a free laminar circular vortex ring (Izutsu & Oshima 1990). Immediately after the maximum downward velocity or the peak velocity on the center line $(-v_o)_{max}$ reaches twice the standard at $t=14.8$ms, when the cross-linked circulation appears on the $y-z$ plane, it decreases until $t=16.4$ms, when the vorticity level 0.125 begins to be cross-linked. Then the position of the maximum downward velocity moves apart from the center line. The maximum downward velocity on the center line continues to decrease monotonously until $t=19.2$ms and the return flow region is swept away from the $x-z$ plane. On the contrary, $(-v_z)_{max}$ expelled from the center line increases again until it reaches the same of $t=14.8$ms. At this moment, $t=18$ms, the vorticity level 0.25 begins to be cross-linked, and from $t=19.2$ms, at halfway for the first cross-

linking and unlinking, the maximum downward velocity begins to decrease quickly so that the sweeping phase of the cross-linking and unlinking is finished by $t=22$ms when the maximum downward velocity $(-v_z)_{max}$ has the bottom value as shown in Fig. 16. On the other hand, the maximum upward velocity on the center line $(v_o)_{max}$ is quickly increases after $t=19.2$ms. By this moment, the maximum downward velocity or the maximum downward momentum appears around $x/R_o=1$ and $y/R_o=1.7$ as shown in Fig. 15.

From these results, the first cross-linking progresses certainly and non-reversibly by the rising driving force of the original near segments pressed harder against each other. The pressure narrows the return flow region and the same flux is kept by the acceleration of the return flow and enlargement of its area. However after the acceleration reaches the limit twice the initial state, it cannot hold the amount of the return flow within the controlled region so that it makes the breach outside the ring to dispose of the overflowed fluid. Once the breach is made, this process is forced to progress towards the finishing state at a breath

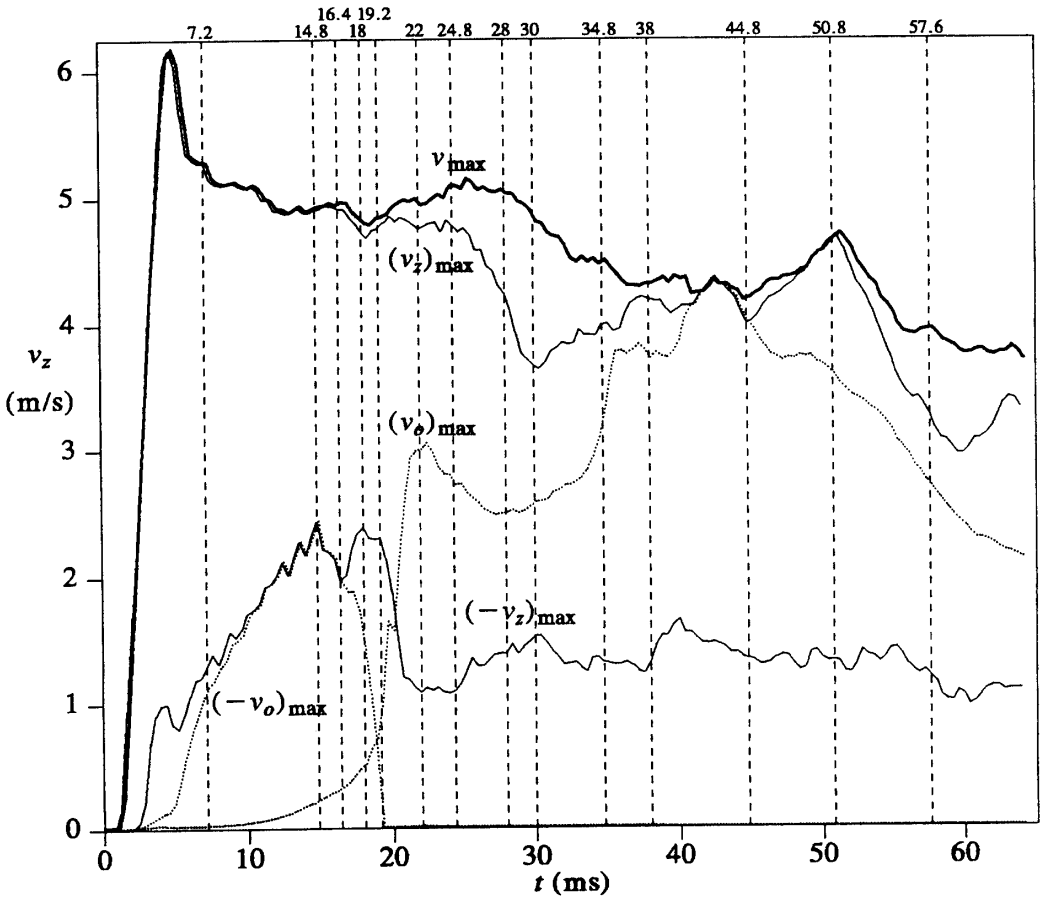

Fig.16 Changes of maximum upward and downward vertical velocities $(v_z)_{max}$ and $(-v_z)_{max}$, peak velocities on the z-axis, $(v_o)_{max}$ and $(-v_o)_{max}$; the thick line indicate the maximum velocity norm at each instant v_{max}.

by means of the still continuous pressing force. It reaches the final state despite the creation of the secondary vortex and the resurrection of the original near segments occurs by vortex stretching.

This process is realized in the vorticity field by the rapid growth of the new vorticity and rapid falloff of the original vorticity. It can be said that the vorticity in the cross-linked segments is transported from the original near segments and no vorticity cancellation is recognized in the adjoining zone. The reason is that the time scale for cancellation is much longer than that for cross-linking and unlinking. The time required in the sweeping phase is 7.2ms observed by 93.75% circulation level. Being observed by the 25% vortex tube level, that is, the core level of the vortex tube, it is only 5.6ms. In the case of the 12.5% vortex tube level it becomes 7.6ms. However the vorticity norm levels observe much shorter time scale such as 2.4ms in the 25% level and 4.8ms in the 12.5% level as written in Table 4.

Figures 17(a) and (b) show the positions of the original far and near center positions, $(x_{c,f}, z_{c,xf})$ and $(x_{c,n}, z_{c,xn})$, as well as the cross-linked far and near center positions, $(y_{c,f}, z_{c,yf})$ and $(y_{c,n}, z_{c,yn})$. In these figures, the z position of the original near center $z_{c,xn}$ is decelerated as it approaches and is pressed to the other near section, and that of the cross-linked far center $z_{c,yf}$ does not easily advance until the 'sweeping rise' phase is finished. On the other hand, around the moment that the first cross-linking and unlinking is almost completed, the original far segments adjoin each other to decelerate and their ascent is stopped and begins to retreat downwards. It is also understood from the plots of the upward velocity of the original far segment, $U_{z,xf}$ in Fig. 18, in which the large deceleration of it is observed and gives even the negative value. This gives an important point for understanding why the second cross-linking fails, and this is discussed in the last subsection. It is clearly presented that the inward velocity of the original far section $U_{x,f}$ is quickly accelerated during the finishing phase of the first cross-linking and unlinking to form the saddle shape of the united vortex ring and that the cross-linked far section is forced downward during the beginning of the first cross-linking due to the large locally induced velocity caused by the powerful original near segments. In this figure, the upward velocity of the centroid for the entire rings U is referred by the thick line for comparison with the velocity of each segment. The initial velocity of the original vortex rings is known as approximately 1.83m/s, so that another Reynolds number of the original vortex ring can be defined as

$$Re_v = \frac{RU}{\nu}, \tag{18}$$

where R is the radius of the vortex ring, and gives the result 1150 at $t=7.2$ms. This Reynolds number gives the smallest evaluation of the reference Reynolds number Re_o, the Reynolds number based on the circulation Re and the Reynolds number based on the traveling velocity Re_v.

(a)

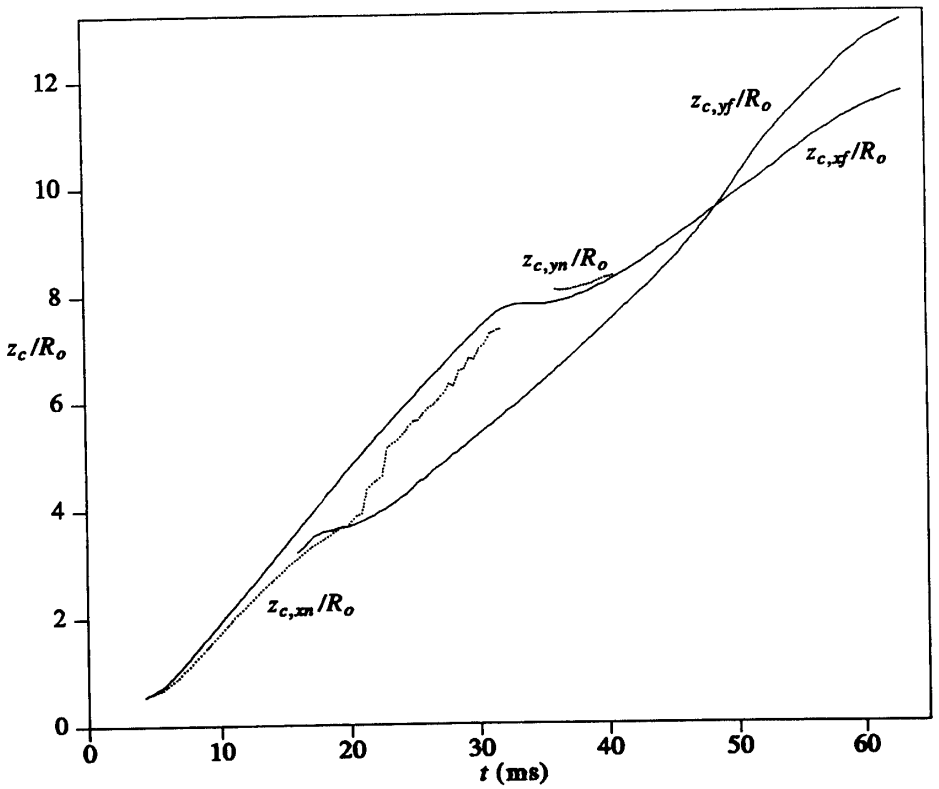

(b)

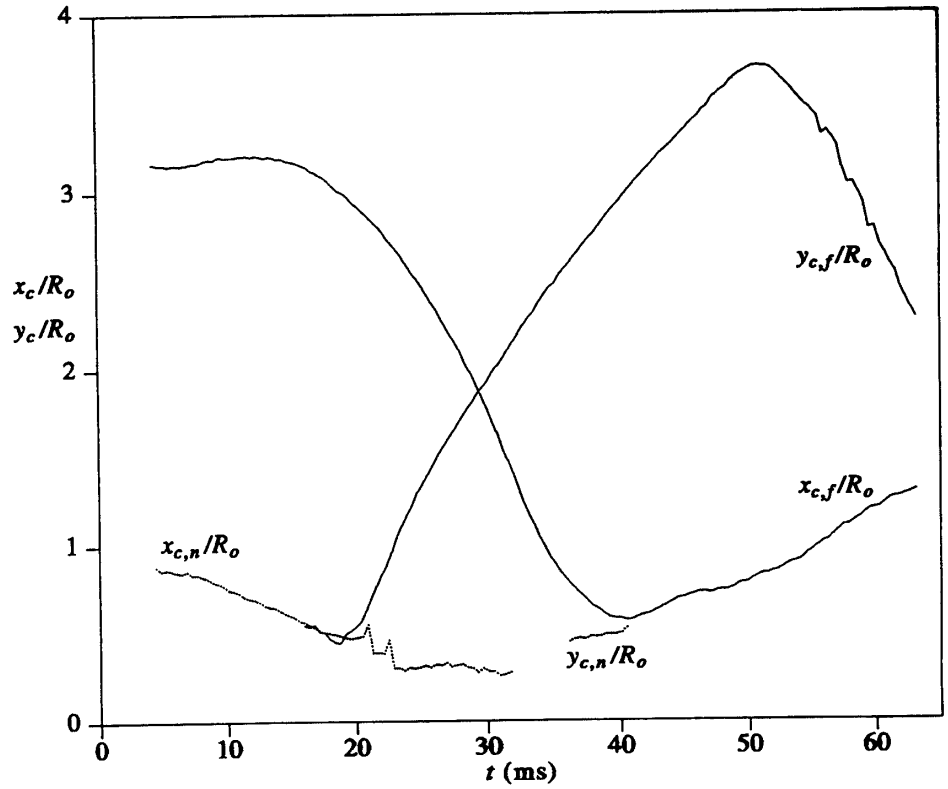

Fig.17 Centers of the original far and near sections on the $x-z$ plane as $(x_{c,f}, z_{c,xf})$ and $(x_{c,n}, z_{c,xn})$, and of the cross-linked far and near sections on the $y-z$ plane as $(y_{c,f}, z_{c,yf})$ and $(y_{c,n}, z_{c,yn})$ are plotted respectively, normalizing by the orifices radius R_o.

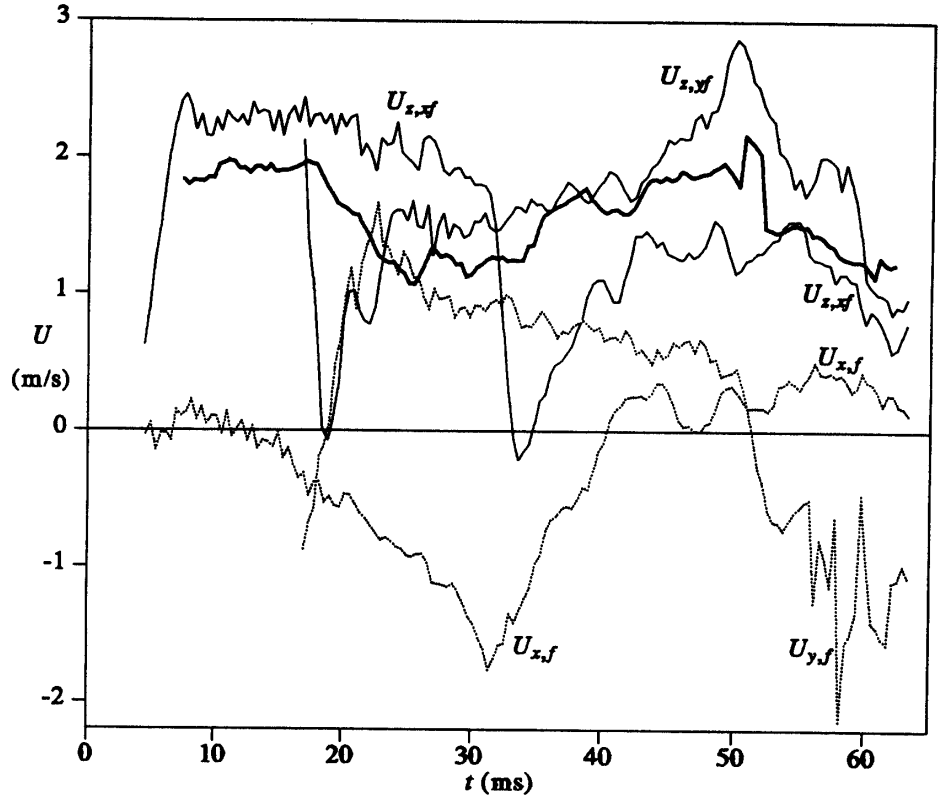

Fig.18 Velocities at centers of the original far section on the $x-z$ plane and cross-linked far section on the $x-z$ plane ($U_{x,f}$, $U_{z,xf}$) and ($U_{y,f}$, $U_{z,yf}$); the thick line indicates the traveling velocity of the centroid of the whole vorticity.

3.4 Fluid material and vortex tubes

In this subsection, what can be visible in direct flow visualizations is discussed in more detail in comparison with the vorticity distribution or vortex tubes. Figure 19 is the directly observed Schlieren pictures placed upper in front views and placed lower in side views. Although it is impossible to take a top view picture by this method, these Schlierens integrated the vertical density gradient from $y=-\infty$ through $y=\infty$ in the front view and from $x=-\infty$ through $x=-\infty$ in the side view result in observation, as the knife edge is set parallel to the x-axis in the front view and to the y-axis in the side view. Although these direct flow visualizations make the images of the uniting vortex rings and seem to show the behavior of the vortex rings, these pictures can show only the behavior of the fluid material and cannot reveal the vorticity fields nor vortex tubes. Therefore, there are several important differences between the direct flow visualizations and the vortex tubes as follows. The beginning moment of the first cross-linking and unlinking is later than that shown by the vorticity cross-linking and unlinking, and the finishing moment of it is also later than that shown by the vorticity fields. The pictures from $t=34$ through 46ms indicate the existence of the 'cap' over the united vortex ring which gradually shrinks to the center line. It is not

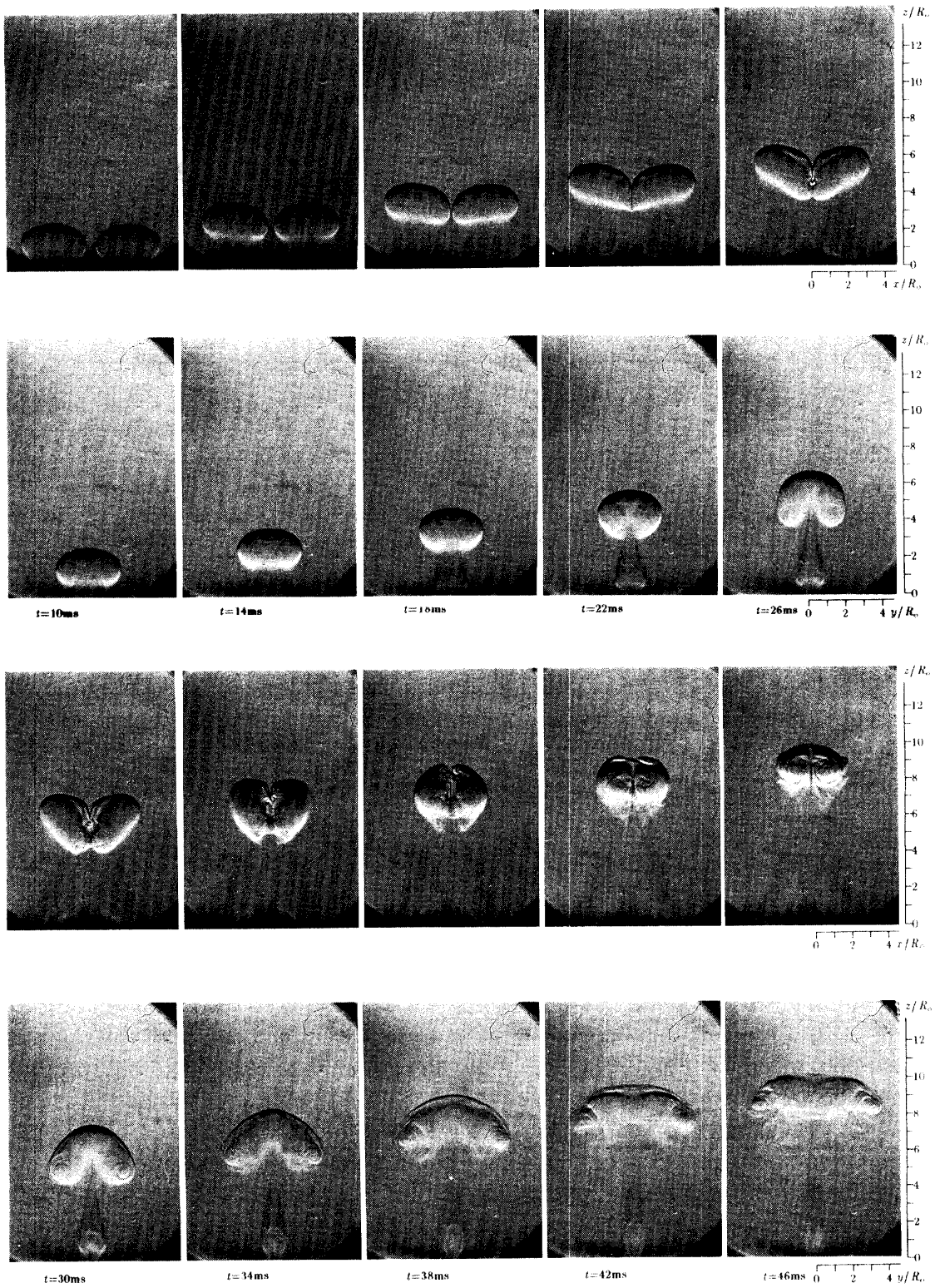

Fig.19 Schlieren images visualized by carbon dioxide fed into the primary jet as the front and side views; the streaks integrated the vertical density gradient in the whole flow region can be observed.

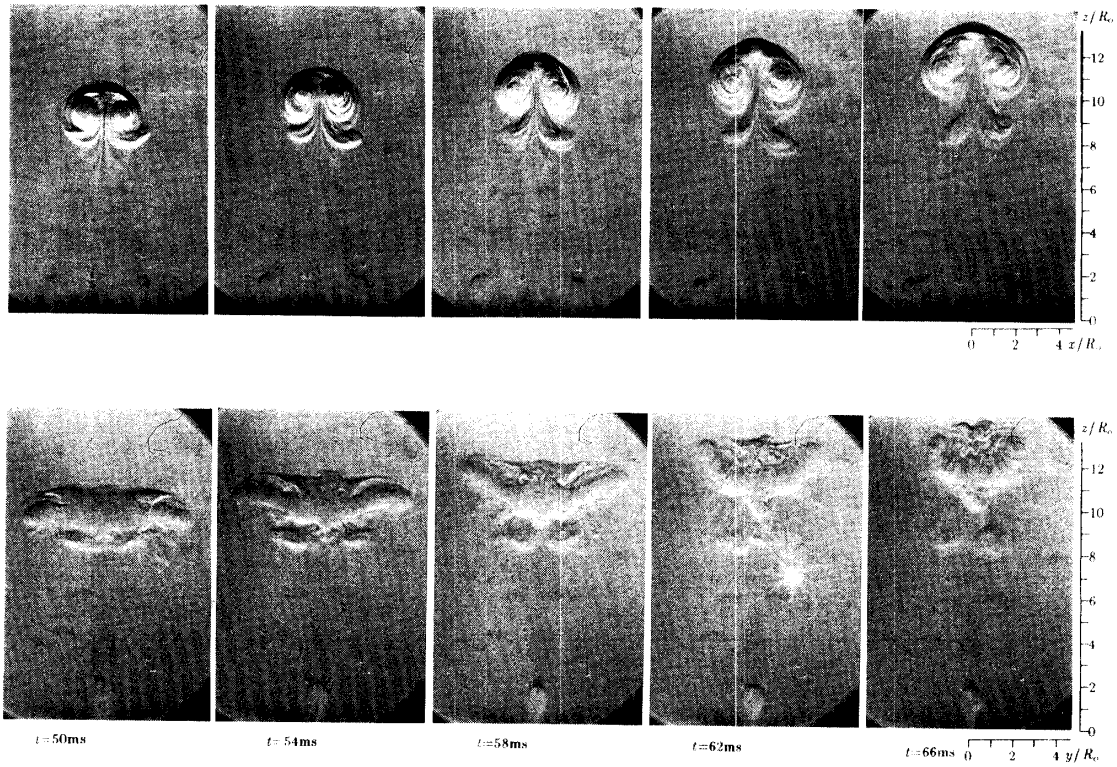

Fig.19 (Continued)

recognized on the vorticity fields. The directly observed deformation of the united vortex ring seems to be stronger than that of the vortex tubes. The pictures at $t=50$ and 54ms show the 'tail' structure growing under the united vortex ring and such the structures are not clear in the vorticity display, however the vorticity 'dripping' around $t=46$ms is observed near the cross-linked far segments in both the direct visualization and the vorticity field. The second cross-linking is mostly pushed on around $t=38$ms in the vorticity field but in the direct visualization it seems to happen around $t=46$ms.

The above mentioned differences are due to that the vorticity field, which is the rotation of the velocity field at each instant, not coinciding at all with the concentration of the fluid material, which is only the result of the transportation caused by the velocity field including the diffusion effect. By integration of the velocity fields with respect to time, the pass lines can be obtained, while the line containing the instantaneous positions of the fluid particles originating at the same specified point in space expresses the streak line. The governing equations for the passive tracers are given by

$$\frac{dx}{v_x(x, y, z, t)} = \frac{dy}{v_y(x, y, z, t)} = \frac{dz}{v_z(x, y, z, t)} = dt, \tag{19}$$

where, t is the variable. Therefore, the simultaneous equations,

$$\frac{dx}{dt}=v_x(x, y, z, t), \frac{dy}{dt}=v_y(x, y, z, t), \frac{dz}{dt}=v_z(x, y, z, t), \text{ (20a,b,c)}$$

can be integrated for each passive tracer, which is firstly located in the initial vortex ring of $t=10$ms. All passive tracers can exactly follow the velocity at their position. The initial condition for each passive tracer in the present study is given at $t=10$ms as the passive tracers are uniformly distributed inside the vortex tube specified by the lower limit ω_o. Therefore, this computation is equivalent to obtain the behavior of the entire fluid material region which is distributed within the vortex ring bounded by the specified outer ring radius. The lower limit vorticity is taken as 0.125 or 0.25 of the maximum vorticity norm, and the spatial discretization of the initial tracers is performed with the third of the enhanced mesh size. After the low pass filtering technique same as the method described in the data processing is adopted two times, the envelope including all tracers is computed and displayed in Fig. 20.

The first cross-linking begins at the nearest segments on the center line, although the vorticity cross-linking starts at the position apart from the z-axis. It is shown in the differences between the plots of $t=18$ms in Fig. 11 and $t=16$ and 18ms in Fig. 21. Figure 21 presents the iso-surfaces of level 0.125 and 0.25 same as those of Fig. 20, in which the form is drawn within the primary quadrant together with the top, side and front views on the right upper, left lower and right lower plots, respectively. The surface with solid lines indicates the outer side of the original material and that of dotted lines does the inner side. The moments of the beginning of the cross-linking and the finishing or stopping of the unlinking are also obtained in Table 4, and both the start of the cross-linking and the end of the unlinking are delayed in comparison with those of the vorticity field or the vortex tubes. In particular, the first cross-linked part exists on the center line and never spreads out easily like the cross-linked far segments of the vortex tube. It remains a dense sphere region and is elongated as an arciform bridge from a cross-linked far segment to the other side as shown in the plots of $t=22$ through 30.4ms in Fig. 20. A part of the initial fluid material is left behind widening the 'tail' toward the bottom near the orifice. This tail is definitely observed by the Schlieren picture of $t=22$ms and never appears in the vorticity field. That is, although the vortex ring makes no vorticity dropping behind it, the fluid material, which follows the velocity field, is partly left behind the vortex ring together with the fluid material supplied from the orifice. It is significant that this tail part has no vorticity. Because of the accumulation of fluid material around the z-axis, the neutral point, in the first cross-linking phase, the first unlinking of the original fluid material on the original near segments is delayed about 5ms.

The united vortex ring of fluid material displayed at $t=30.4$ and 34.8ms is more distorted compared with the vortex tubes in Fig. 12. The cap recognized from $t=34$ to 46ms in Fig. 19 is caused by the elongated fluid material on the united vortex ring observed at $t=30.4$ through 51.2ms in Fig. 20. The part

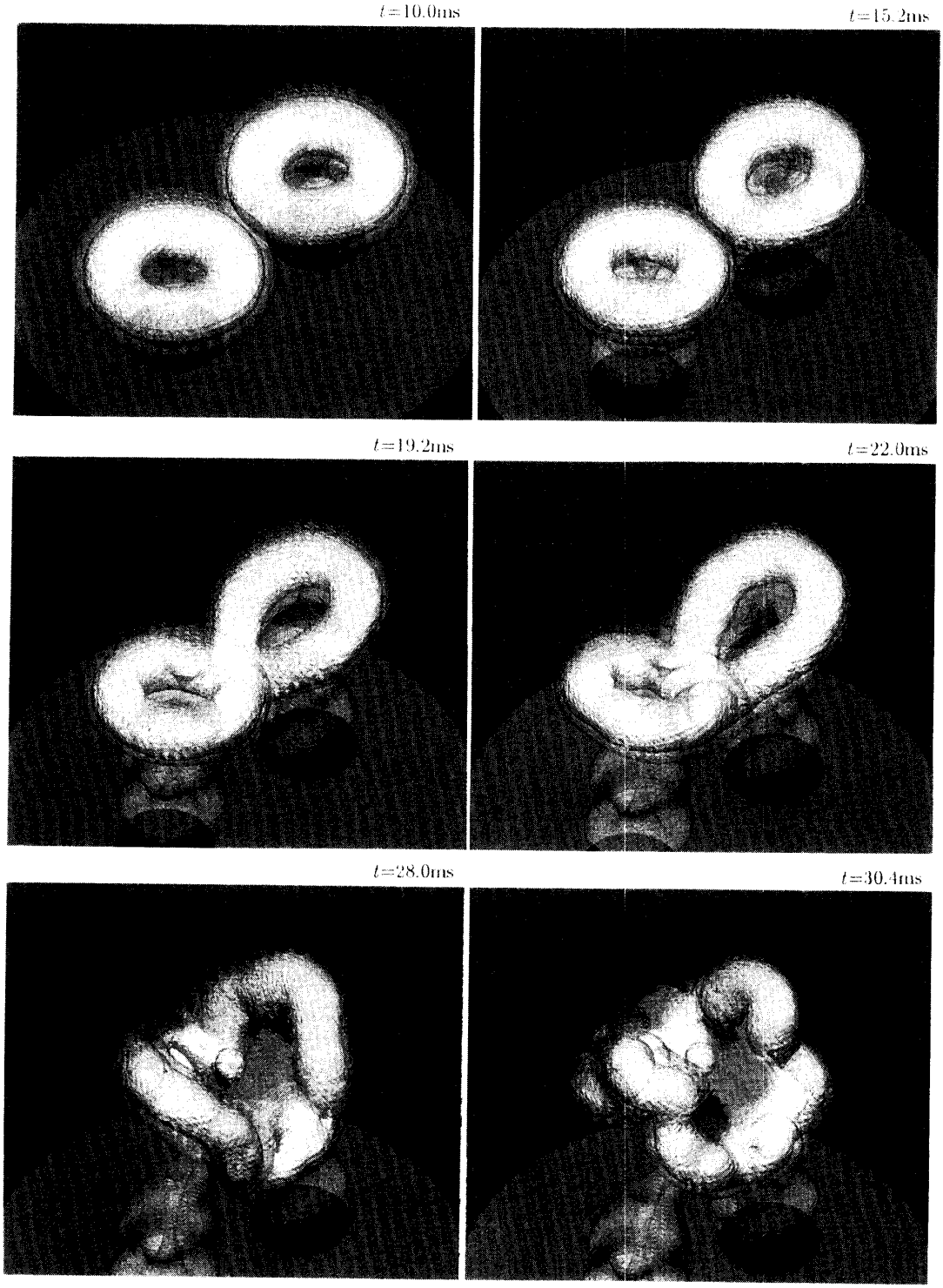

Fig.20 Evolution of the computed envelopes of the fluid material initially distributed inside the vortex tube of $t = 10$ms; the surfaces corresponding to the initial vortex tubes of which specified lower limit level are 0.125, 0.25, 0.5 and 0.75 of the maximum vorticity norm at each instant ω_{max} are drawn white, yellow, orange and red, respectively.

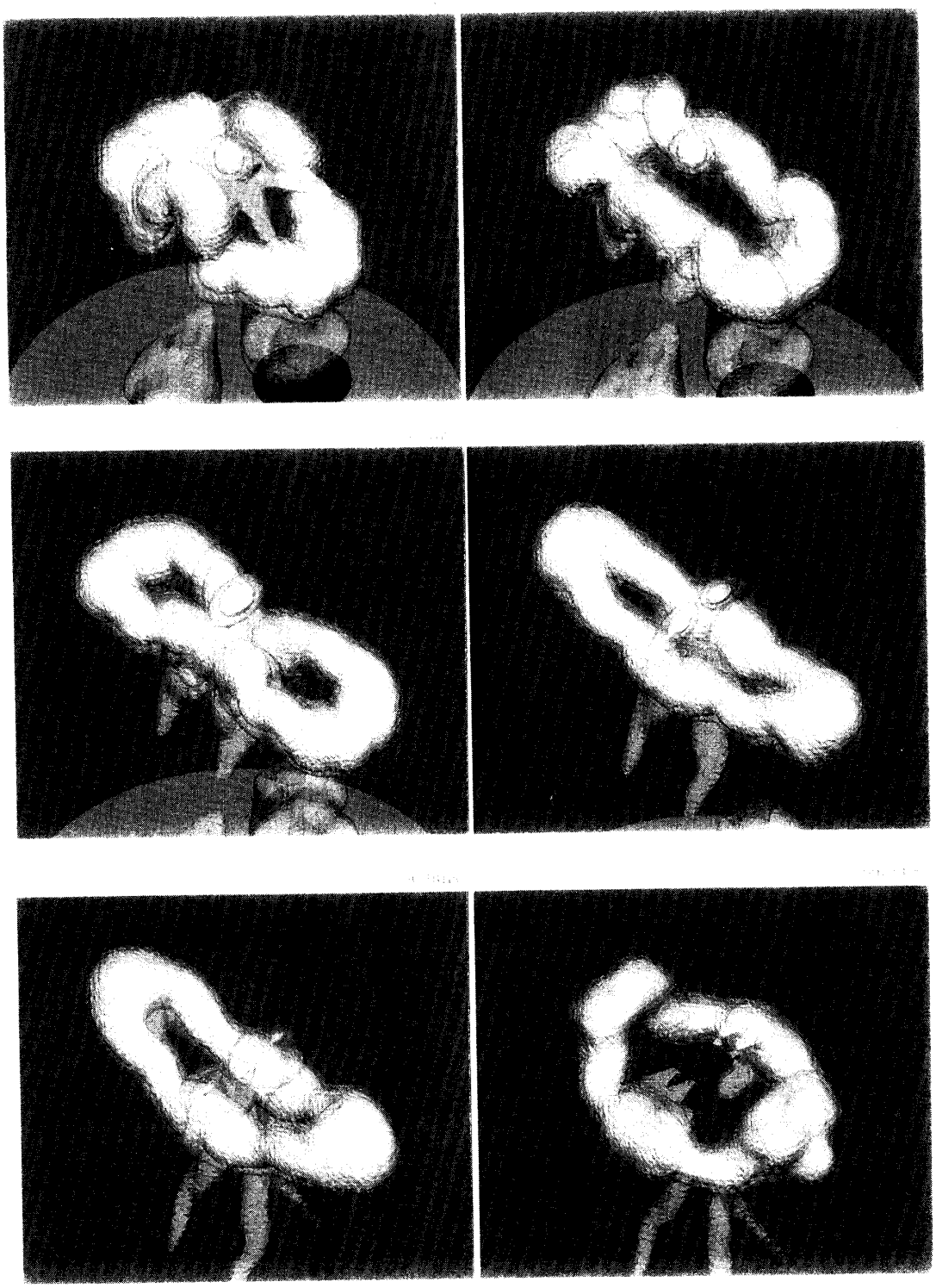

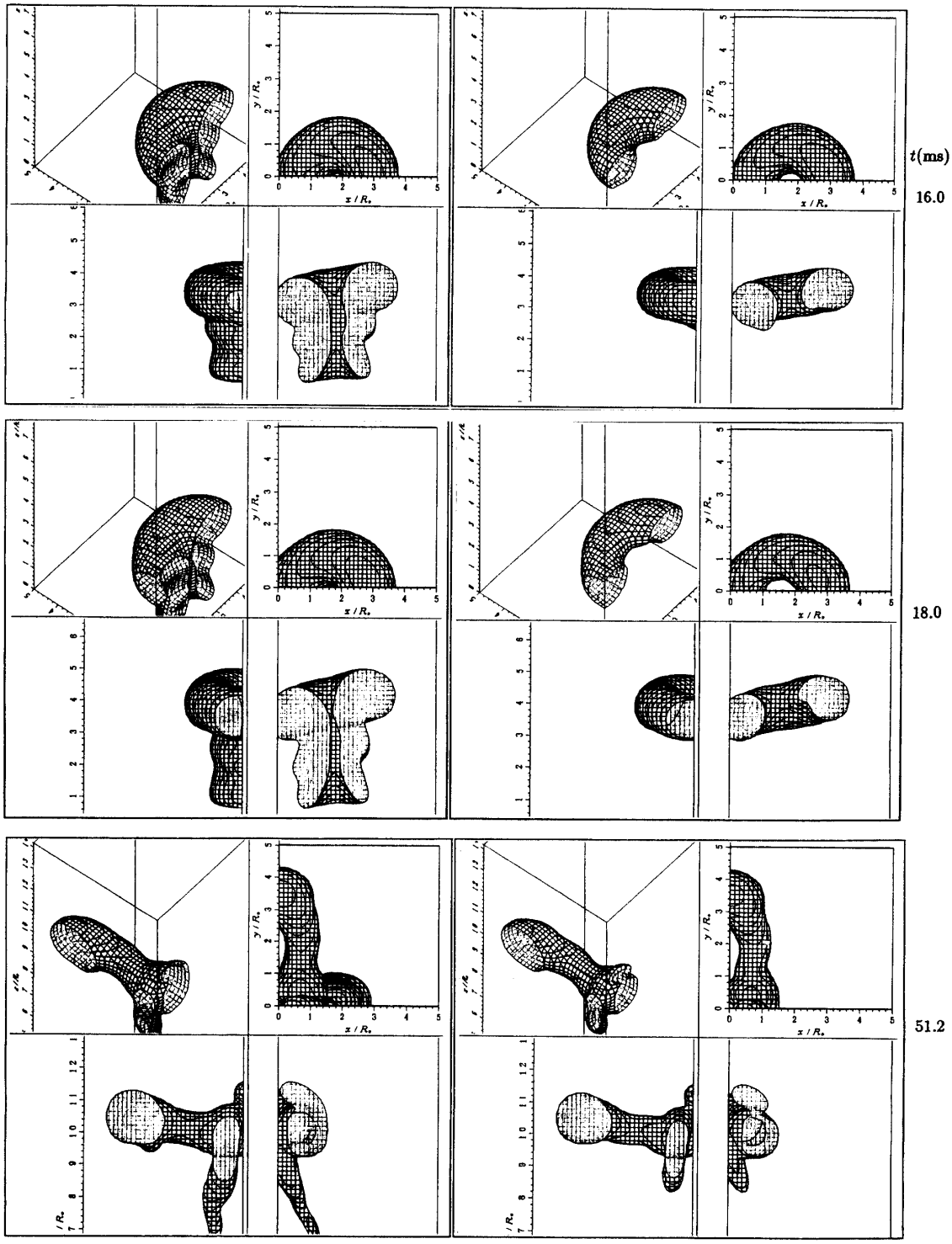

Fig.21 Fluid material of the level (a) 0.125 and (b) 0.25, which means the same as in Fig. 20, are drawn within the primary quadrant together with the top, side and front views on the upper right, lower left and lower right plots, respectively; the surface with solid lines indicates the lower value side and that of dotted lines does the higher.

Table 4. Time scale from the started instant of cross-linking through the finished instant of unlinking.

regulation		circulation	vorticity		vortex tube		fluid material	
level		93.75%	12.5%	25.0%	12.5%	25.0%	12.5%	25.0%
1st cross-linking	from t(ms)=	15.0	16.2	17.8	14.2	15.4	14.6	15.8
1st unlinking	till t(ms)=	34.8	21.0	20.2	21.8	21.0	27.0	25.8
2nd cross-linking	from t(ms)=	34.8	35.8	—	35.0	36.6	43.0	43.0
2nd unlinking	till t(ms)=	44.8	40.2	—	49.8	42.6	60.6	57.8

outside the dense sphere region is gradually disappears and the dense part on the center line finally entrained into the adjoined original far segment as shown at $t=44.8$ and 51.2ms in Fig. 20. From $t=38$ms another tail is dripped and extended downward from four points under the united vortex ring. This phenomenon originates in the largely bent segments of fluid material as shown at $t=34.8$ and 38ms of Fig. 20. These dripped parts adjoin each other and are elongated as the original far segments are approaching one another, and it reaches the peak situation of $t=44.8$ms, when the united vortex ring seems to be split partly into two new vortex rings. This situation is also denoted by the plot of $t=51.2$ms in Fig. 21. Here, it is to be noted that the vortex tubes indicate no splitting at $t=44.8$ms as shown in the plot of $t=44.8$ms in Fig. 12 and that the vortex tubes make the second cross-linking only around $t=38$ms. Thus, the differences of recognition for the second cross-linking and unlinking between the vorticity fields and the pursued fluid material become more than 8~15ms as written in Table 4. There is only the rapidly declining vorticity within the tails which are recognized under the united vortex ring in Fig. 19 after $t=38$ms.

The accumulated dense material around the center line is entrained into the adjoining original far segments as they begin to spread out, and another arciform bridge structure linked between the original far segments is recognized from $t=$ 44.8 through 56ms in Fig. 20 as well as in the Schlieren pictures in Fig. 19. The vorticity dripping which happened from $t=50.8$ms results in the quick reduction of the total enstrophy as well as the total energy of the united vortex ring, which is plotted in Fig. 22, where the energy E and the enstrophy Q within the whole measured region are defined by

$$E(t)=\frac{1}{2}\int\frac{v(x, y, z, t)^2}{R_o{}^3 v_{MAX}{}^2}dxdydz, \tag{21a}$$

$$Q(t)=\frac{1}{2}\int\frac{\omega(x, y, z, t)^2}{R_o v_{MAX}{}^2}dxdydz, \tag{21b}$$

in the primary quadrant and they are normalized by the maximum velocity norm v_{MAX} and the orifice radius R_o. The helicity on the primary quadrant is also calculated from

$$H(t)=\int\frac{\omega(x, y, z, t)\cdot v(x, y, z, t)}{R_o{}^2 v_{MAX}{}^2}dxdydz. \tag{21c}$$

The enstrophy decreases both in the sweeping phase of the first cross-linking and unlinking and in the decay phase by the dripping after the second cross-linking and unlinking. The former is caused by the rearrangement of the vorticity field, however the latter decrease is due to vorticity dripping behind the united vortex ring, in which the dripped vorticity is forced to be reduced quickly. Therefore, no energy decrease is recognized during the former decrease of the enstrophy, however a large energy decline happens in the latter decay phase. On the other hand, the helicity shows the rate of inclination of the vortex tubes, denoting that the original far segment is placed above the other part before $t=45$ms while the cross-linked far segment is ahead of the original far segment after $t=45$ms.

The ascending velocity of the centroid U in Fig. 18 shows that although it decreases during the sweeping phase of the first cross-linking and unlinking, it continues to increase after that and reaches the maximum velocity around $t=$ 51.2ms. This acceleration is initiated by both the upward velocities of both the original far and cross-linked far segments. These radical accelerations result in the large distortion around the four middle points between the original far and cross-linked far segments and the vorticity dripping consequently occurs from these points.

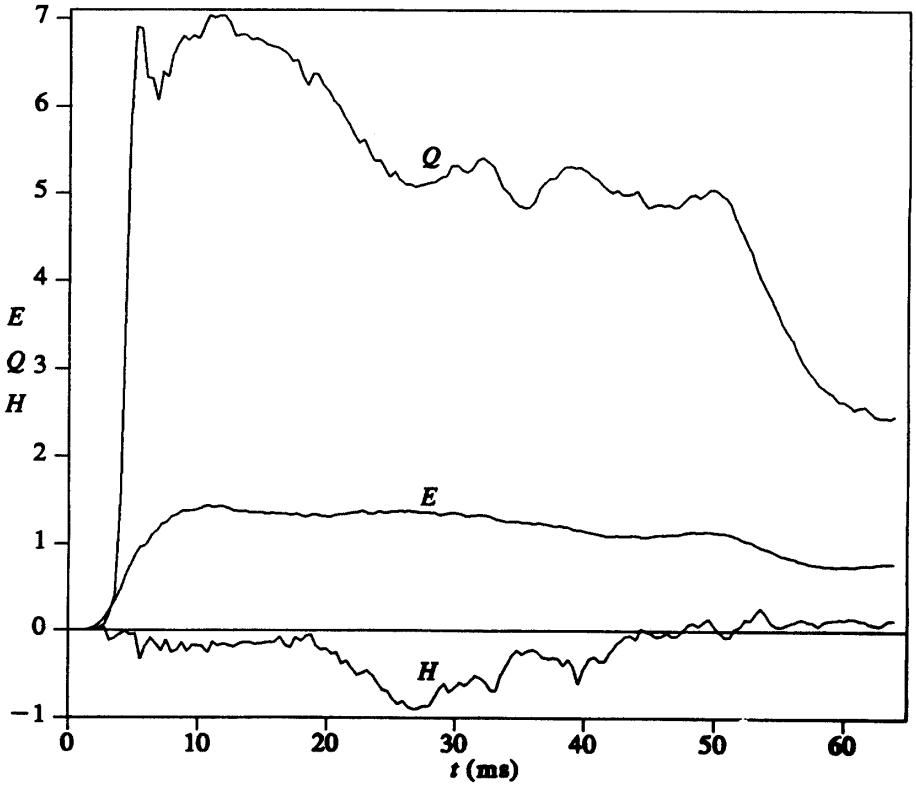

Fig.22 Energy E , enstrophy Q and helicity H totaled in the primary quadrant.

3.5 Second cross-linking

The difference between the first cross-linking and unlinking and the second cross-linking and unlinking is explained, and showing how the first cross-linking and unlinking are successfully finished while the second ones fail. Around $t=38$ms the adjoined segments of the original far segment receive the down force due to the induced velocity between them just as the adjoined original near does, while they get another driving force caused by the induced velocity due to its local curvature. In the first cross-linking and unlinking term, the driving force acting on the original near segment is upward and inward (towards the center line), so that it is pressed to the other original near segment and is forced to ascend upward. Therefore the original near segment gradually decreases its upward velocity so that the ring inclines more and more to get harder pressing force. This continuous and increasing pressing force is the motive power for the first cross-linking and unlinking which never fail. On the other hand, in the second cross-linking and unlinking term, the driving force due to the local curvature on the original far segment is acting downward and inward. Because the induced velocities between the original far segments are also downward, their parts are decelerated much more. This downward force is strong enough to make the segment begin to retreat, while the pressing force towards the other original far segment is coming from the inclination of the united vortex ring so that the adjoined part is in the top position and the already cross-linked far segments are in the lowest. Contrary to the retreating original far segments, the cross-linked far segments are radically accelerated by their induced velocities due to their local curvatures. As a result, the driving force of the inward component rapidly decreases as the inclination decreases by the cross-linked far segments proceeding faster. After the united vortex ring is level with the orifice plane, the opposite angle of inclination results the outward driving force, in which no pressing force exists. It is known from these features that the rapidly decreasing pressing force leads to the failure of the second cross-linking and unlinking, if the initial pressing force and its holding time is not enough to finish the whole cross-linking and unlinking. This can be said to be the diverging point whether the united vortex ring again splits or not, and it is expected to be concerned with the final approaching angle. It can be said that the second cross-linking and unlinking are a 'negative' process depending on the initial condition, contrary to the first cross-linking and unlinking which are a 'positive' one. The feature for the failure of the second cross-linking and unlinking is also confirmed in the velocity field of Figs. 14 and 16. It is shown in Fig. 14 that the driving force on the original far segments being pressed each other is temporary and the newly appeared velocity gradient on the $y-z$ plane is soon weakened. The maximum upward velocity on the center line in Fig. 16 shows that its acceleration around $t=34.8$ms is not enough to reach the critical point which ensures the successful cross-linking and unlinking.

4. Concluding Remarks

Uniting two laminar circular vortex rings consist of the processes of; (1) formation, isolating and approaching, (2) first cross-linking and unlinking, (3) second cross-linking and unlinking, (4) decay, when the united vortex ring finally becomes an elliptic vortex ring. The process in each term can be described by the changes of 93.75% of the circulations on the planes of symmetry. Two vortex rings are formed by shedding the accumulated vorticity generated along the orifice edges in the formation phase, and they begin to propagate as the primary vortex rings by being isolated from the trail vorticity, which gains the circulation of up to 17% of that of the initial vortex ring. As soon as the vortex rings are formed, they begin to approach each other due to their mutual induced velocities. Immediately after the original near segments are adjoined on the $y-z$ plane, the sweeping rises of two cross-linked vortex tubes between the original near segments are observed, simultaneously the sweeping falloff of the vorticity in the original near section is performed. This positive cross-linking and unlinking are successfully finished after the secondary vortices appear and disappear. Since the continuous and increasing driving force on the adjoined original near segments which are pressed against each other narrows the return flow region in their gap, it is accelerated to reach the critical instant when the gap cannot hold the whole flux. The return flow overflows outward to create another velocity gradient, which is observed as the sudden appearance of new concentrated vorticity regions. The vorticity distributed on the original near segments is transported to the cross-linked segments in this way, which can be said to push the return flow in the gap out. Once this breach is made, this process is forced to finish swiftly.

The second cross-linking and unlinking process starts immediately after the first cross-linking and unlinking finish. It is negative and stops due to the monotonously decreasing driving force on the adjoined original 'far' segments in the united vortex ring. It is expected to depend on the initial condition such as the final approaching angle. The cap and tail parts in the behavior of fluid material appear but not in the vorticity field. The differences among the vorticity field, the vortex tubes and the behavior of the material fluid tend to confuse the real phenomenon, such as the beginning of the cross-linking, the ending of the unlinking, the deformation of the united vortex ring and the behavior of the trail, cap and tail. They also lead to disagreement about the interpretation of the progress and situation of the second cross-linking and unlinking besides its shape.

Secondary vortex tubes appear with up to 13% of the initial circulation nearby the segments propagating with a large inward or outward velocity due to the distortion of the local velocity field. The time scale for the cross-linking and unlinking can be obtained by watching the behavior of the computed vortex tubes and considerably differs from that by the vorticity norm, or, by the fluid material observed in the direct flow visualization. The time required for the

sweeping phase of the first cross-linking and unlinking is only 5.6ms in the vortex core level, which is much shorter than 19.8ms in the 93.75% circulation level.

References

Ashurst, Wm. T. & Meiron, D. I. 1987 Numerical study of vortex reconnection. *Phys. Rev. Lett.* **58**, 1632.

Chen, H. L. 1991 Numerical study on vortical flows. Dr. Thesis, The university of Tokyo.

Fohl, T. & Turner, J. S. 1975 Colliding vortex rings. *Phys. Fluids* **18**, 433.

Ishii, K., Hussain, F., Kuwahara, K. & Liu, C. H. 1989 The dynamics of vortex rings in an unbounded domain. *Advances in Turbulence 2*, Springer Verlag Berlin, Heidelberg 51.

Izutsu, N. & Oshima, Y. 1990 *Private communication.*

Kerr. R. M. & Hussain, F. 1989 Simulation of vortex reconnection. *Physica D* **37**, 474.

Kida, S., Takaoka, M. & Hussain, F. 1989 Reconnection of two vortex rings. *Phys. Fluids A* **1**, 630.

Leonard A. & Chua K. 1989 Three-dimensional interactions of vortex tubes. *Physica D* **37**, 490.

Melander, M. V. & Zabusky N. J. 1988 Interaction and "apparent" reconnection of 3D vortex tubes via direct numerical simulations. *Fluid Dyn. Res.* **3**, 247.

Noguchi, T. 1986 Three-dimensional interactions of vortices with finite core. M. S. Thesis, University of Tokyo.

Oshima, Y. & Asaka, S. 1975 Interaction of two vortex rings moving side by side. *Nat. Sci. Rep. Ochanomizu Univ.* **26**, 31.

Oshima, Y. & Asaka, S. 1977 Interaction of two vortex rings along parallel axes in air. *J. Phys. Soc. Japan* **42**, 708.

Oshima, Y. & Izutsu, N. 1988 Cross-linking of two vortex rings. *Phys. Fluids* **31**, 2401.

Saffman, P. G. 1990 A model of vortex reconnection. *J. Fluid Mech.* **212**, 395.

Schatzle, P. R. 1987 An experimental study of fusion of vortex rings. Ph. D. thesis, California Institute of Technology.